Sofia Daniela Silva Machado

Green synthesis of bioactive nanoparticles in algae from North Portugal
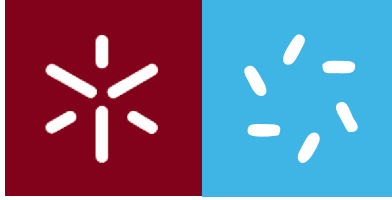
Green synthesis of bioactive nanoparticles in algae from North Portugal

Sofia Machado

UMinho | 2019

Outubro de 2019

Universidade do Minho
Escola de Ciências

Sofia Daniela Silva Machado

Green synthesis of bioactive nanoparticles in algae from North Portugal

Master Thesis
Master in Molecular Biology, Biotechnology and
Bioentrepreneurship in Plants

Work developed under supervision of
Andreia Ferreira de Castro Gomes

and
Maria Carmen Rodríguez-Argüelles

Outubro de 2019

Declaração

Nome: Sofia Daniela Silva Machado

Endereço eletrónico: sofia.smachadoutlook.com

Telefone: +351932903268

Número do Bilhete de Identidade: 14399078

Título:

Green synthesis of bioactive nanoparticles in algae from North Portugal

Orientadores:

Professora Doutora Andreia Ferreira de Castro Gomes

Professora Doutora Maria Carmen Rodríguez-Argüelles

Ano de conclusão: 2019

Designação do Mestrado: Biologia Molecular, Biotecnologia e Bioempreendedorismo em Plantas

EMBARGO TOTAL DA TESE DURANTE DOIS ANOS APÓS DEFESA PÚBLICA PARA PERMITIR ESCRITA E SUBMISSÃO DE MANUSCRITO PARA PUBLICAÇÃO EM REVISTA INTERNACIONAL.

Universidade do Minho, ____/____/_____

Assinatura: _Sofia Machado_____

I. AGRADECIMENTOS

II. STATEMENT OF INTEGRITY

I hereby declare having conducted this academic work with integrity. I confirm that I have not used plagiarism or any form of undue use of information or falsification of results along the process leading to its elaboration.

I further declare that I have fully acknowledged the Code of Ethical Conduct of the University of Minho.

University of Minho, 31ˢᵗ October 2019

Signature: _Sofia Machado_____

III. ABSTRACT

In recent years, the development of efficient green methods for synthesis of metal nanoparticles has emerged as an eco-friendly alternative for production of well-characterized nanoparticles instead of chemical processes which are more expensive and pollutant. Among the diverse techniques, plants, bacteria and fungi can be used in the synthesis.

In a project focused on the green synthesis of new nanomaterials with biomedical application, the brown marine algae *Cystoseira baccata* was chosen as target specie for obtaining gold nanoparticles with antitumor activity. An efficient method for the biosynthesis of gold nanoparticles using *C. baccata* extract was developed by the research group led by Professor Maria C. Rodríguez-Argüelles (Vigo University, Spain) however further studies were necessary to clarify effects of the green synthesized gold nanoparticles in advanced *in vitro* and *in vivo* models to confirm them as effective, but non-toxic tools, for cancer therapies.

Interestingly, a different species of *Cystoseira* is found in specific areas of coastal Northern Portugal, the *Cystoseira tamariscifolia*. Gold nanoparticles were produced using this specie, guided by the same protocol used with *C. baccata* and, similar toxicity and bioactivity studies were performed in order to understand if different members of the genus are capable of producing similar nanoparticles through green biosynthesis and evaluate its biocompability. To assess cell viability, MTT assay was performed, for cell proliferation the wound-healing assay was carried out and lastly, for *in vivo* evaluation, ZET assay was executed. The use of zebrafish embryos allowed to obtain toxicology data in complex organisms quickly and efficiently, permitting to conclude on multiple parameters at once.

Finally, the results from the two algae extracts and derived nanoparticles were compared.

Keywords: bioactivity, *Cystoseira*, gold nanoparticles, green synthesis, toxicity.

IV. RESUMO

Nos últimos anos, o desenvolvimento de métodos eficientes de "síntese verde" para a síntese de nanopartículas metálicas emergiu como uma alternativa ambientalista para a produção de nanopartículas bem caracterizadas, em vez dos processos químicos atuais que são mais caros e poluentes. Dentro das várias técnicas, plantas, bactérias e fungos podem ser usados na síntese.

Num projeto focado na biossíntese de novos nanomateriais com aplicação biomédica, a alga marinha castanha *Cystoseira baccata* foi escolhida como espécie-alvo para obtenção de nanopartículas de ouro com atividade anti tumoral. Um método eficiente para a biossíntese de nanopartículas de ouro usando o extrato de *C. baccatta* foi desenvolvido pelo grupo de pesquisa liderado pela professora Maria C. Rodríguez-Argüelles (Universidade de Vigo, Espanha), contudo estudos adicionais são necessários para esclarecer os efeitos das nanopartículas de ouro produzidas por síntese verde podem ter em modelos *in vitro* e *in vivo* como alternativas eficazes mas não tóxicas para terapias contra o cancro.

Curiosamente, uma espécie diferente de *Cystoseira* é encontrada em áreas específicas da costa norte de Portugal, a *Cystoseira tamariscifolia*. Nanopartículas de ouro foram produzidas nesta espécie, utilizando o mesmo protocolo usado com a *C. baccata* e, estudos semelhantes de toxicidade e bioatividade foram realizados para entender se todos os membros do género são capazes de produzir nanopartículas semelhantes com a biossíntese verde e avaliar a sua biocompatibilidade.

Para avaliar a viabilidade celular, foi realizado o ensaio MTT, para a proliferação celular, foi realizado o ensaio "wound-healing" e, por fim, para avaliação *in vivo*, foi realizado o ensaio ZET. O uso de embriões de peixe-zebra permitiu obter dados toxicológicos em organismos complexos de maneira rápida e eficiente, permitindo concluir vários parâmetros ao mesmo tempo.

Finalmente, foram comparados os resultados dos dois extratos de algas e as suas respetivas nanopartículas.

Palavras-chave: bioatividade, *Cystoseira*, nanopartículas de ouro, "síntese verde", toxicidade.

VI. ABBREVIATIONS

ATCC American Type Culture Collection

Au@CB Gold nanoparticles derived from *Cystoseira baccata* extract

Au@CT Gold nanoparticles derived from *Cystoseira tamariscifolia* extract

AuNPs Gold Nanoparticles

CB *Cystoseira baccata*

CT *Cystoseira tamariscifolia*

CTH hexane extract

DMSO Dimethyl sulfoxide

DPPH 2,2-Diphenyl-1-picrylhydrazyl

FTIR Fourier-Transform Infrared Spectroscopy

GAE Galic Acid Equivalents

h_{pf} hours post-fertilization

KFG Keratinocyte Growth Factor

L_T body length

MTT 3-[4,5-dimethylthiazol-2-yl]-2,5-diphenyltetrazolium bromide

NPs Nanoparticles

OECD Organisation for Economic Co-operation and Development

SPR Surface Plasmon Resonance

UV–vis spectroscopy Ultraviolet–Visible spectroscopy

TEM Transmission Electron Microscopy

TPC Total Phenolic Content

ZET Zebrafish Embryo toxicity Test

VII.   FIGURE INDEX

VIII. TABLE INDEX

I. INTRODUCTION

1. Green synthesis

Green synthesis is the common designation given to synthetic routes which use relatively non-toxic, biodegradable and low cost chemical products to synthesize nanomaterials, having as their primary source or initiator route a biological organism or parts thereof (organs, tissues, cells, biomolecules or metabolites)[1]. The application of green chemistry into green nanotechnology enables the development of safer and cleaner technologies that decrease health risks and strengthen care for the environment. In the end, this method involves the design of products and processes that can decrease or eradicate hazardous substances and minimize waste production[2].

Physical and chemical synthesis have an intensive energy consume and can sometimes involve the use of toxic compounds. The generation of residues harmful to health and the environment result in high energy consumption on generally complex and multi-step routes, while biological techniques are cost-effective, clean, non-toxic and ecologically correct. In this method, high temperatures, pressures, and energy levels are not required[3]. The biological synthesis pathway has been carried out, above all, through the use of bacteria, fungi and plants[4].

Plants contain functional biomolecules that actively reduce metal ions and this process can happen in a single-step[3]. In addition, they act as stabilizing agents for nanoparticles. Interestingly, all parts of plants can be efficiently used to synthesize nanoparticles, such as leaves, stems, seeds, fruits, latex, etc. The plant's dead and dried biomass can also be used for the successful synthesis of nanoparticles. Even bioactive compounds isolated from plants such as polyphenols, alkaloids, flavonoids and terpenes have been shown to synthesize nanoparticles[4]. These nanoparticles are commonly very stable, with various shapes and sizes and their rate of synthesis is fast in comparison with nanoparticles produced by other organisms[5]. Plant materials are renewable, therefore are easily available and the use of its extracts does not require sophisticated laboratories for cell cultures[3].

Similar to plants, there are algae that being the largest photoautotrophic group of microorganisms are the potential source for an array of secondary metabolites, pigments and proteins[6]. There are algae that are known to hyperaccumulate heavy metal ions and possess an exceptional capability to remodel them into more malleable forms. Therefore these are great "nanobiofactories" once having a faster doubling time, are easily scalable and well developed systems, cells can be readily disrupted, easily harvested, low cost and large-scale synthesis and nucleation and crystal growth are accelerated due to the presence of negative charge on the surface of the cell[6]. Thus, seaweed phytochemicals, including hydroxyl, carboxyl,

and amino functional groups, can serve both as effective metal-reducing and capping agents to provide a robust coating on the metal nanoparticles in a single step[7].

These main features make this innovative method more attractive and a potential option for many applications such as, medical, industrial, electronic devices, sensors, cosmetics, pharmaceutical, agriculture and bioremediation[6].

2. Seaweeds

Seaweeds or macroalgae are the most familiar types of protists, which are eukaryotic, photosynthesizing multi-cellular organisms that lack the specialized structures and reproductive mechanisms characteristic of true plants. There are three types of macroalgae that are distinguished by the different types of photosynthetic pigments found in their cells: **green algae** (Phylum Chlorophyta), **brown algae** (Phylum Phaeophyta), and **red algae** (Phylum Rhodophyta).

Nowadays, seaweeds represent an unlimited source of the raw materials used in pharmaceutical, food and cosmetics industries. This is possible due to its well-known characteristics, as functional food for their richness in lipids, minerals and certain vitamins, and also several bioactive substances like polysaccharides, proteins and polyphones, with potential medicinal uses against cancer, oxidative stress and other degenerative diseases[7].

Cystoseira baccata (CB) and *Cystoseira tamariscifolia (CT)* are two species of brown algae from the same genus that differ in geographic distribution, morphology and possibly content of secondary metabolites. In this study, CB and CT extracts were used to produce gold nanoparticles through an environment-friendly route.

2.1 Cystoseira genus

Cystoseira is a genus of marine brown algae composed of about 40 species[8]. It is represented by a few species in Atlantic coast, it has diversified in a large manner across the Mediterranean Sea, whereas were described more than 30 taxa. As a result of an intense adaptive radiation, the Mediterranean *Cystoseira* algae are found in diverse biotopes, from the surface to 100 m deep.

Every species have the same organization plan, with a base, one or various erect axis, and a system of branches of several orders and reproductive organs (receptacles) intercalated or terminals on the branches.

Cystoseira are perennial algae that renew their branches seasonally. The fall of these can be partial or total; in the latter case, only the base subsists during the seasonal rest, usually in the fall or winter.

Cystoseira species are composed of brown algae that have longer longevity[9].

The main criteria of determination are those related to the base of the thallus, its bushiness character, the aspect of the apices, the shape of the branches, the presence of characteristic thickening in its base , the existence of branches of last level, short and spiny, called ''leaves'' (by analogy with the superior plants), and finally, the location and the appearance of the receptacles[10]. Thus, the identification of a *Cystoseira* is often difficult[10].

This genus produces a wide variety of secondary metabolites (e.g. terpenoids, steroids, phlorotannins, phenolic compounds, carbohydrates, fatty acids, pigments, vitamins) that are associated with pharmacological properties, such as antioxidant, anti-inflammatory, cytotoxicity, anticancer, cholinesterase inhibition and anti-diabetic activities but also antibacterial, antifungal and anti-parasitic activities[8]. A review[8] that have studied the isolated compounds of algae from *Cystoseira* genus, and their respective therapeutic potential, showed that these algae contain compounds with different biomedical potential, providing an extensive list of natural isolated structures that could be used as scaffolds to the design of novel leads for pharmacological purposes. Most bioactive metabolites found were lipids followed by terpenoids (including meroterpenoids), steroids, carbohydrates, phlorotannins, phenolic compounds, pigments and vitamins. From terpenoids, isololiolide, was isolated from *C. tamariscifolia*, and proved to be cytotoxic against gastric cancer cells and selectively cytotoxic on human hepatocellular carcinoma cells comparing with non-tumoral human fibroblasts; fucosterol, a steroid present in *Cystoseira tamariscifolia*, showed to have antileishmanial activitiy; also the study of three *Cystoseira* species, (that includes, *C. tamariscifolia*) by HPLC reported the occurrence of different phlorotannins. This compound is known to have anti-bacterial and antifungal properties. It also showed anti-inflammatory activity, inducing a marked decline of nitric oxide production in lipopolysaccharide-stimulated macrophages, especially *C. tamariscifolia* extract; mannitol, a carbohydrate, also found in *C. tamariscifolia* is used in numerous cosmetic and pharmaceutical applications because of its hydrating and antioxidant properties; pigments, like carotenoids, β-carotene and astaxanthin, known for their antioxidant and anti-inflammatory properties, were found in *C. baccata*. When evaluated for its antiproliferative effect on human T-cell leukemia cells, these compounds displayed a mild inhibitory activity.

2.1.1 Cystoseira baccata

C. baccata (**Figure 1**) is an algae of olive colour, not bright that can reach more than 2 m in length. Set to the substrate for a disk, which comprises a cylindrical main axis that is narrowed at the apex, which makes the branches fall stand more or less zigzag, top to bottom[11]. The main ones present secondary

branches, the closest to the base are flattened (similar to small stitches), with 1-5 mm in width[11]. In the summer, it presents numerous elliptical or rounded air-cysts, sometimes forming rosaries, interspersed in the stem[11]. The receptacles are stretched, cylindrical, simple or bifurcated and sometimes with some thorns. It is a monoic species[11].

CB lives on the rocks of the infralittoral and in the lakes of the lower coast, both on the semi-dry and protected coasts. It appears abundantly scattered on the beaches in the North Atlantic, from the British Isles to the coasts of Mauritania. It is used in the production of alginates, and also as fertilizers[11].

Figure 1- *Cystoseira baccata.*

2.1.2 *Cystoseira tamariscifolia*

C. tamariscifolia (**Figure 2**) is a species of olive green colour, when under water it has reflections of deep blue colour, which makes it more or less easy to recognize. It is a robust algi, 60 cm long. It is attached to the substrate by a basal disc from which arises a cylindrical main axis that branches repeatedly in all directions[11]. The secondary branches are much divided, and cover themselves with small spine-like branches, which they often call leaves. In the summer it presents air-cysts near the receptacles, which are small at the apex and wider at the base[11].

It inhabits the large pools of the lower littoral and infralittoral, both on exposed and semi-exposed coasts and extends across Atlantic Europe to Mauritania[11]. It can be abundant in waters of high ecological status in the Mediterranean, on intertidal rocky shores[12].

It is used in the production of alginates, and also as fertilizers[11].

Figure 2- *Cystoseira tamariscifolia.*

3. Nanomtechnology

3.1 Nanomaterials

In the first place, it is necessary to introduce the concept of nanotechnology. There are very different definitions, but one of the most accepted is: "Nanotechnologies are the design, characterisation, production and application of structures, devices and systems by controlling shape and size at nanometre scale"[13]. This size range is defined to be from a nanometer (10^{-9} m=1 nm or a little smaller) to 100 nm or a little larger (up to several hundred nanometers)[13,14].

There are different ways of classifying nanomaterials (**Figure 3**), the most common been based on their composition or on their dimensions. As regards their dimension, they can be divided into[15]: **0D**: all dimension are nanometrics: nanoparticles, quantum dots, fullerenes, liposomes and dendrimers; **1D**: only one dimension in the nanoscale: nanorods, nanowires, nanofibers and nanotubes; **2D**: two dimensions in the nanoscale: films, plates, graphene and quantum well; **3D**: none of the dimensions are in the nanoscale, but however it is formed from nanoscale grains or crystals.
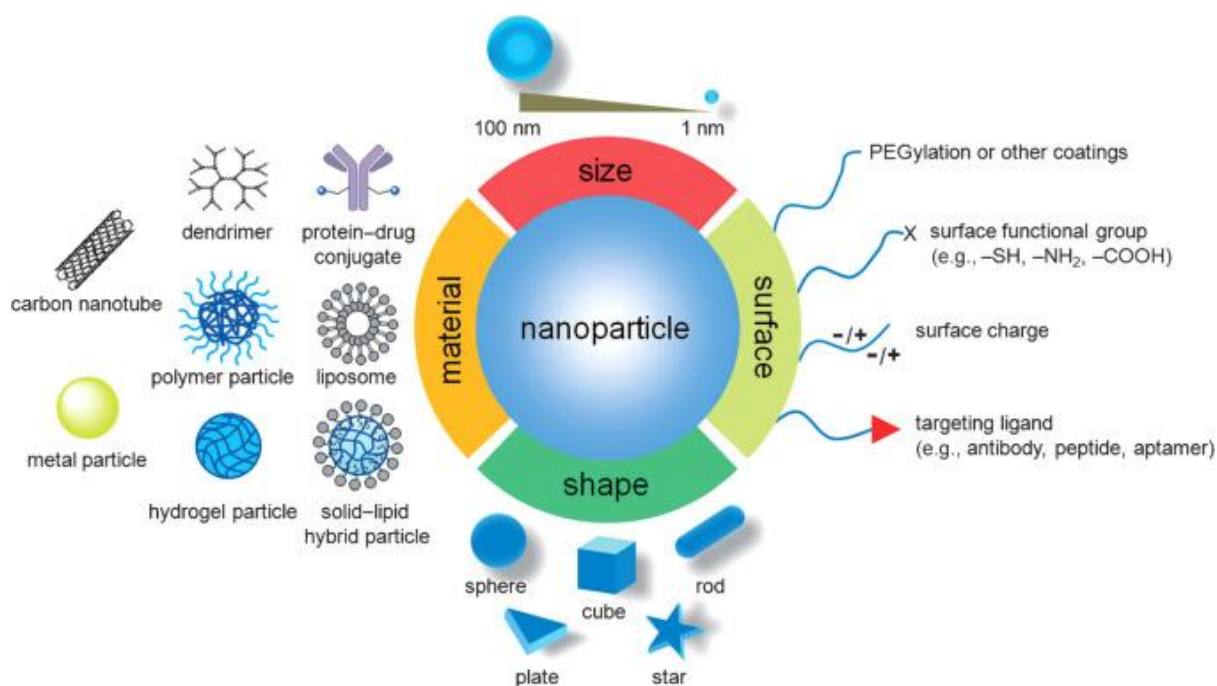
Figure 3- Illustrations of biophysicochemical properties of nanoparticles[16].

3.2 Metal nanoparticles

Metal nanoparticles are made of metal precursors. These NPs are considered important, owing to their unique particle size (small sizes, high surface area) and shape-dependent physiochemical (tunable optical, physical, and chemical properties) and biological (noncytotoxicity) properties[2,17] that allows them to have potential applications in the development of new technologies for biomedicine, as optoelectronic devices, biological sensors, targeted drug delivery systems, and also as catalysts[18].

Gold nanoparticles are also extensively used in the biotechnology and biomedical fields due to their large surface area and high electron conductivity, and have been proven safe and much less toxic as drug delivery agents[2]. Also, gold nanoparticles have shown antitumor activity onto several cancer cells (induce apoptosis in HL-60 cancerous cells, MCF-7 breast cancer cells, A-549 human lung cancer and others) because these usually respond resonantly to the magnetic field, which varies with time, allowing them to transfer enough toxic thermal energy to tumour cells as hyperthermic agents[2].

3.3 Applications of nanoparticles

Nanoparticles have many useful and meaningful applications such as **imaging and diagnosis** reflecting ability to detect, quantify, and display molecular and cellular changes that occur *in vitro* and *in vivo*; **drug delivery** that is seriously relevant in the therapeutic modulation of effective drug dose and disease control[19]. Targeted encapsulated drug delivery using NPs is more effective for improved bioavailability,

19

minimal side effects, decreased toxicity to other organs, and is less costly[20]. NP-based drug delivery is feasible in hydrophobic and hydrophilic states through variable routes of administration, including oral, vascular and inhalation; **anticancer therapy**, as nowadays conventional anti-cancer treatments are scarce in specificity to target killing of tumour cells, may induce severe systemic toxicity, and produce drug resistant phenotypic growth[21]. An exciting potential use of nanotechnology in cancer treatments is the exploration of tumour-specific thermal scalpels to heat and burn tumours; ultimately, in **gene therapy**, since conventional medicine uses viral vectors that are associated with adverse immunologic, inflammatory reactions, and diseases in the host[22]. Using NPs, a normal gene is inserted in place of an abnormal disease-causing gene using a carrier molecule and some studies have demonstrated less cytotoxicity in these cases[23].

3.4 Nanoparticles toxicity

Effective potential of **nanoparticles toxicity** has not been completely addressed. Most research focuses on the toxicity of chemically or physically synthesized metal oxide nanoparticles[24]. There are relatively few reports that characterize the nanotoxicity of biogenic metal oxide nanoparticles. Based on published papers, the clear determination of the similarities and differences, in terms of toxicity, of metal oxide nanoparticles obtained by traditional methods and by biogenic routes can be considered complex[24]. This complexity is due to the different routes of nanoparticles synthesis, their different size, presence or absence of capping molecules, diverse kinds of toxicity evaluation tests, and lack of deeper studies of nanotoxicity of biogenic nanoparticles. Therefore, the potential toxic effects of biogenically obtained nanoparticles should be investigated further[25]. Therefore, the toxicity of the nanoparticles made by a green route will be thoroughly evaluated.

4. Zebrafish
4.1 Taxonomy and morphology

The zebrafish (Hamilton, 1822) is a derived member of genus *Danio*, of family Cyprinidae. It is named for the five uniform, pigmented, horizontal, blue stripes on the side of the body, which are reminiscent of a zebra's stripes, and which extend to the end of the caudal fin. Its shape is fusiform and laterally compressed, with its mouth directed upwards. Males have a torpedo-shaped, with gold stripes between the blue stripes; females have a larger, whitish belly and silver stripes instead of gold. Adult females exhibit a small genital papilla in front of the anal fin origin[26]. The zebrafish can grow to 6.4 cm in length, although it seldom grows larger than 4 cm in captivity[26]. Its lifespan in captivity is around two to three

years, although in ideal conditions, this may be extended to over five years.

4.2 Life cycle

In **Figure 4** it can be observed the life cycle of zebrafish. It develops rapidly from a one-cell zygote that sits on top of a large yolk cell. Gastrulation begins approximately 6 hours post fertilization (h_{pf}), hatching of about 48 h, as a free-swimming larvae. It reaches sexual maturity around 3 months of age[27].
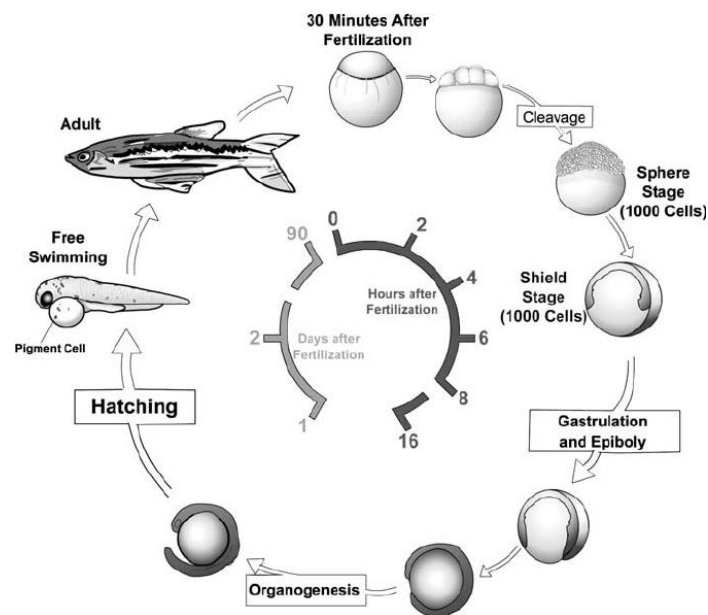
Figure 4- *Zebrafish life cycle*[53].

4.3 Zebrafish as a model for in vivo assays

Zebrafish is a complex organism that provides a fast, easy, inexpensive and an ethical method compared to rodent models that have stringent regulations and ethical constraints and that are also more costly. Additionally, the Zebrafish Embryo toxicity Test (ZET) was considered an acute fish toxicity test by OECD (Organization for Economic Co-operation and Development)[28]. It is a good model because of their small size, large numbers, optical clarity and rapid external development, no other vertebrate model can match zebrafish embryos when it comes to high-throughput phenotyping[29]. Particularly, the use of zebrafish embryos allow to obtain toxicology data in complex organisms quickly and efficiently, permitting to conclude on multiple parameters at once.

5. Objectives

In recent years, nanotechnology has emerged as a science with a growing number of applications. Among the developed nanomaterials, gold nanoparticles present physico-chemical properties that attract the

attention of several researchers all over the world. Current chemical and physical techniques make possible the synthesis of gold nanoparticles with different sizes and shapes, whereas in almost all chemical methods, the use of toxic and expensive reagents is required[30]. For this reason, the development of green methods for the synthesis of gold nanoparticles is an area of great interest and large potential growth. It is a simple and one-step technique that uses non-toxic and renewable materials. Furthermore, it is more economic.

Algae were selected because these synthetize bioactive substances, like polyphenols with potential medicine uses against cancer, oxidative stress and another degenerative diseases[31]. Thus, seaweed phytochemicals, including hydroxyl and carboxyl groups can serve as metal-reducing and capping agents[32].

Cystoseira genus was chosen because it produces a wide variety of secondary metabolites (like phenolic compounds, carbohydrates and vitamins) that are associated with pharmacological properties, such as antioxidant or anti-inflammatory activities[33]. In a work focused on the update of chemical entities and biological activities of the *Cystoseira* genus, antibacterial, antifungal and anti-parasitic activities as antimalarial and antileishmanial were also reported, but less often than the other activities above mentioned [8].

Our group in Vigo have made NPs from *C. baccata* and prove that these had a strong cytotoxicity activity against colon cancer cell inducing apoptotic activation by extrinsic and mitochondrial pathway, and a great biocompatibility with a normal cell line. However, further studies should be carried out to clarify the effects derived nanoparticles using *in vivo* models.

C. tamariscifolia was chosen because it belongs to the same genus as *C. baccata*, inhabits in the north Portuguese coast and also, researches from Vizetto-Duarte et al., showed interesting bioactivity and cytotoxicity against cancer cells. A work showed that between three species of the genus *Cystoseira*, *C. tamariscifolia* was the one with more phenolic content and a potent selective cytotoxic effect against hepatocellular carcinoma cells, especially its hexane extract (CTH). Moreover, CTH reduced cell proliferation and inhibited cell growth through apoptosis induction[34]. Likewise, in another work, a compound named isololiolide, was isolated from CTH, which showed anti-tumoral activity against hepatocarcinoma cells, through the induction of apoptosis, by altering the expression of proteins, important to the apoptotic cascade. No cytotoxicity on non-tumoral human fibroblasts under the same conditions was proved[35].

In this study, after synthesis of gold nanoparticles using an eco-friendly approach, these were tested for their bioactivity and biocompability of both extracts and gold nanoparticles in order to inquire and compare

the results between the algae and, finally, to study which biomolecules are involved in the synthesis of the nanoparticles.

Ultimately, the major goal is to prove that production of nanoparticles using biological entities has the potential to deliver new sources materials that are stable, nontoxic, cost effective and environmentally friendly.

II.   MATERIALS AND METHODS

1.   Methodologies for preparation and characterization of extracts and nanoparticles

1.1 Preparation of the extract

Thalli of live bunches of *Cystoseira tamariscifolia* (CT) were collected at the lower intertidal rocky shore in the NW coast of Portugal (N 41 47.858' W 008 52.423'). Samples were either immediately processed or frozen at -24 °C until treatment. Tetrachloroauric acid trihydrate (99.9 %) was purchased by Merck. All other used reagents were of analytical grade and the ultrapure water (18.2 MW cm at 25 °C) was used throughout the experiments.

At the beginning, the seaweeds were thoroughly rinsed with ultrapure water to remove seawater, sand and associated biota. Fragments of seaweeds were cut into fine pieces and placed in a double neck balloon connected to a refrigerant. Ultrapure was added in a proportion of 0.2 g/mL and the solution was then boiled at reflux during 15 min. The extract was thus centrifuged in a Beckman coulter Microfuge 16 at 4500 rpm for 10 min, and the supernatant was filtered. Part of the obtained extract was stored at 4 °C and the remnant was frozen at -4 °C until further treatment (**Figure 5**).

Figure 5-Scheme of the preparation of the aqueous extract.

1.2 Preparation of the nanoparticles

Gold nanoparticles were synthesized using *CT* aqueous extract as reagent. Briefly, different volumes between 50 and 150 μL of $HAuCl_4$ 0.01 M were slowly added to CT extract. The solution was kept at room temperature while being stirred for 2 h. The progress of Au@CT (nanoparticles made from CT extract) synthesis was observed every 10 s by UV–vis spectroscopy, on a Jasco Spectrometer V-670, and the reaction took place after a 10-15 min. The reading was performed at 537 nm, and the end point was established when no further change in the surface plasmon resonance peak intensity was observed.

1.3 Characterization

The formation of spherical and stable nanoparticles was demonstrated by UV–vis spectroscopy, TEM

analysis and zeta potential measurements.

1.3.1 UV-vis spectroscopy

UV–vis spectroscopy refers to absorption spectroscopy or reflectance spectroscopy in the ultraviolet-visible spectral region, which measures the absorption of a beam of light after it has passed through the sample or after reflection from the sample surface, through a spectrophotometer[36].

For spectroscopy purposes, it was chosen to characterize light in the ultraviolet and visible regions in terms of wavelength expressed in nanometres. The range of UV and visible region is 100-400 nm and 400-800 nm, respectively.

UV–Vis spectra were recorded at room temperature, on a Jasco Spectrometer V-670. It was used to measure the reaction time, the phenolic content, the reducing power and the DPPH scavenging of the extracts and the AuNPs (gold nanoparticles).

1.3.2 TEM analysis

TEM is a microscopy technique in which a beam of electrons is transmitted through a specimen to form an image. The specimen is most often an ultrathin section less than 100 nm thick, or a suspension on a grid. An image is formed from the interaction of the electrons with the sample as the beam is transmitted through the specimen. The image is then magnified and focused onto an imaging device, such as a fluorescent screen, a layer of photographic film, or a sensor such as a charge-coupled device[37].

Samples for transmission electron microscopy (TEM) observation were prepared by dropping the nanoparticle suspensions directly onto a Formvar-carbon coated copper grid (TED PELLA 01814-F Carbon Type-B, 400 mesh), and left to dry. TEM images were acquired with a JEOL JEM1010 TEM, operated at 100 kV. All acquisition and data analysis were carried out using Digital Micrograph software by Gatan.

1.3.3 Zeta Potential Measurements

Zeta potential measurements are the potential difference between the dispersion medium and the stationary layer of fluid attached to the dispersed particle. The usual units are volts or millivolts.

The zeta potential is a key indicator of the stability of colloidal dispersions. The magnitude of the zeta potential indicates the degree of electrostatic repulsion between adjacent, similarly charged particles in a dispersion. For molecules and particles that are small enough, a high zeta potential will confer stability, i.e., the solution or dispersion will resist to aggregation[38]. When the potential is small, attractive forces may exceed this repulsion and the dispersion may break and flocculate. So, colloids with high zeta

potential (negative or positive) are electrically stabilized while colloids with low zeta potentials tend to coagulate or flocculate as outlined in the forward **Table 1**.

Zeta potential was obtained through electrophoretic mobility by taking the average of five measurements at the stationary level using a ZetasizerNano S (Malvern Instruments, Malvern U.K.) equipped with 4 mW He−Ne laser operating at a wavelength of 633 nm.

Table 1- Stability guidelines classifying NP-dispersions with Z-potetial values[38].

Z-potential (mV)	Stability behaviour
±0-10	Highly unstable
±10-20	Relatively stable
±20-30	Moderately stable
>30	Highly stable

1.4 Characterization of the functional group of biomolecules

1.4.1 FTIR

The functional group of biomolecules present in *CT* extract and gold nanoparticles were characterized by FTIR.

Regarding sample preparation for the FTIR spectroscopy analysis, the extracts and the gold nanoparticles were placed in an oven at 80 °C until dry. The dried materials were then grinded to a fine powder, and then used to record the spectra by employing the KBr pellet technique. The mixture was compressed into a pellet with a manual hydraulic press. A Jasco FT/IR-6100 spectrophotometer was used at a resolution of 4 cm^{-1} in the range of 4000−400 cm[-1][39].

1.5 Antioxidant Activity

1.5.1 Phenolic content

The content of soluble phenols was measured using a modified Folin and Ciocalteu method[30]. The reduction of the reagent by phenolic compounds forms a blue compound and the absorbance was measured at 720 nm. The results were expressed as gallic acid equivalents (GAE), using a calibration curve over the range of 0.05[-1] mg/mL. All measurements were performed in triplicate and results are expressed as mean ± standard deviation.

1.5.2 Reducing power

The reducing power of *CT* extract and Au@CT were measured following a modified version of the Oyaizu method[30]. In summary, 1 mL of seaweed extract at a concentration of 0.2 g/mL and Au@CT were treated following the protocol previously described. A standard curve was built with ascorbic acid at concentrations between 50 and 400 mg/L and seaweed extract reducing power was expressed as mg of ascorbic acid/g of seaweed. All trials were performed in triplicate and the result was expressed as mean ± standard deviation. Absorbance at 700 nm increased when the concentration of ascorbic acid was raised, indicating higher reductive ability.

1.5.3 DPPH

The free radical scavenging activity of the extracts on 1, 1-diphenyl-2-picryl-hydrazyl (DPPH) was evaluated according to the previously reported method by (Shen *et al.*, 2010)[39] with some modifications. Briefly, a 0.1 mM solution of DPPH in methanol was freshly prepared and 1 mL of this solution was added to 3 mL of the aqueous extracts diluted at a ratio of 1:4. After that, mixtures were shaken vigorously and allowed to stand at room temperature for 30 min. Then, the absorbance was measured at 517 nm using a UV–Vis spectrophotometer. Ascorbic acid was used as the reference (at a concentration range of 2–0.1 mg/L). For blank, 2. 75 mL distilled water, 1 mL of methanol and 250 μL of extract were used and a sample control was also made for each fraction by mixing 3 mL of sample with 1 mL of methanol. Lower absorbance values of reaction mixture indicate higher free radical scavenging activity. The capability of scavenging the DPPH radical was calculated by using the formula.

DPPH scavenging efect (% inhibition)$=(1-\frac{A_s-A_{s0}}{A_b}$), where, A_b is the absorbance of the blank, A_s is the absorbance in the presence of the extract samples and reference and A_{s0} is the sample control. All the tests were performed in triplicate. The effective concentration required to decrease the initial DPPH concentration by 50 % (EC50) was also calculated.

The CB extract and NPs characterization was previously performed and published[30].

2. Methodologies for biological validation

Despite of all nanoparticles advantages mentioned, these can also have unwanted effects, as mentioned above, and therefore, testing their toxicity and bioactivity is of major relevance, which was evaluated using *in vitro* and *in vivo* models.

In vitro nanotoxicity testing, generally, is simple but it is subjected, however, from several obvious shortcomings, such as oversimplified systems and setups, moderately informative and conclusive results,

and limited translational value. Factors such as route of administration, biodistribution, biodegradability, long-term disposition, induction of developmental defects and activation of the compliment and/or immune system are major issues in determining *in vivo* nanotoxicity, and cannot be properly addressed using *in vitro* experimental setups[40]. Therefore, these should be analysed following a complementary perspective.

2.1 Cell lines

The evaluation of toxicity *in vitro* was determined using a human cell line, BJ-5ta and a mouse cell line, L929 (**Figure 6**).
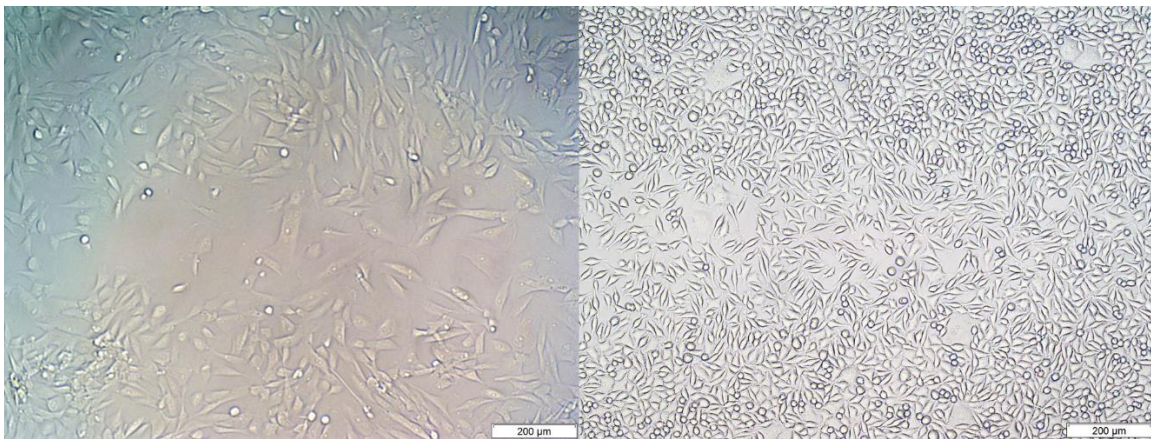
Figure 6- Images of BJ-5ta (on the left) and L929 (on the right) cells.

BJ-5ta cells are fibroblasts immortalized with hTERT of foreskin from a male of *Homo sapiens* species. L 929 cells are fibroblasts of subcutaneous connective tissue (areolar and adipose) from a male of *Mus musculus*. This cell line is a suitable host for transfection.

2.2 *In vitro* Assays

2.2.1 MTT

Cellular metabolism was assessed by tetrazolium-based colorimetric cellular assay (MTT). The (3-[4,5-dimethylthiazol-2-yl]-2,5-diphenyltetrazolium bromide) (MTT) is a cell viability assay often used to determine cytotoxicity following exposure to toxic substances. MTT is a water soluble tetrazolium salt, which is converted to an insoluble purple formazan by cleavage of the tetrazolium ring by succinate dehydrogenase within the mitochondria (**Figure 7**), and it absorbs light at 570 nm. Formazan product is impermeable to the cell membranes, and therefore it accumulates in healthy cells. If the cellular metabolism somehow becomes impaired, the salt will not be metabolized and, as consequence, the

absorption of light will be diminished. In this way, the percentage of cell viability could be estimated by measuring the absorption of the formed crystals.
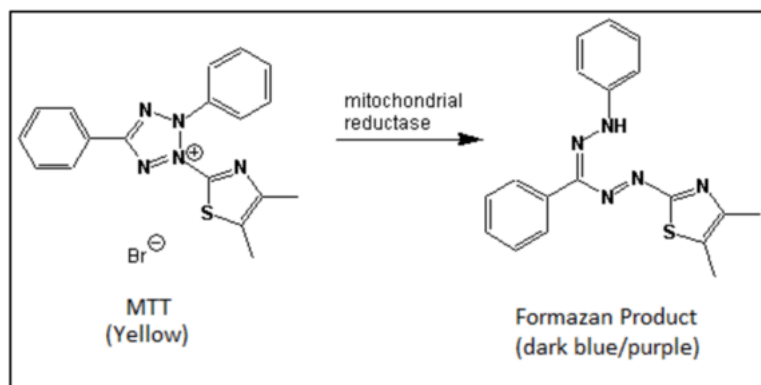
Figure 7- Tetrazolium salt conversion to formazan[41].

Stock solutions (1 g/mL for *CB* and 0.2 g/mL for *CT* extract) were diluted in the respective cell medium, in order to obtain the nominal test concentrations (0.125 g/mL, 0.0625 g/mL, 0.03125 g/mL, 0.0125 g/mL, 0.00625 g/mL and 0.003125 g/mL). Nanoparticles were also diluted from stock solution (0.4 mM) to the pretended test concentrations (12.5 µM, 5 µM, 2.5 µM and 1.25 µM) using cell medium. Cells were seeded into 96 well-microplates at a cell density of 1.2×10^5 (for BJ-5ta cells) and 5×10^3 (for L929 cells) cells/well, and incubated for 24h, at 5% CO_2 and 37 ˚C, incubator (C150 – Binder). After the incubation period, the medium was removed and the cells were incubated with the different concentrations of extracts and NPs, in triplicates. The controls used were: negative control (viability) – cells incubated with fresh medium only; positive control (death) – cells incubated with medium containing 30 % ($^v/_v$) DMSO and H_2O control (12.5%) – cells incubated with medium containing a similar amount of filtered water to that used to prepare the highest concentration of extracts and NPs in use, to ensure that the water absorption by the cells wasn't a toxic factor. Cells were maintained in an incubator with 5 % CO_2, at 37 ˚C for 24 h.

Then, cell viability was assessed after 2 h of incubation with MTT solution (0.5 mg/mL) at 37 ˚C. After incubation, the medium was removed and a fresh etanol:DMSO solution (1:1, ($^v/_v$)) was added to each well to dissolve the developed crystals of formazan. The absorption levels were measured at 570 nm, in the SpectraMax Plus 384 Microplate Reader (Molecular Devices), using etanol:DMSO solution as blank (**Figure 8**).
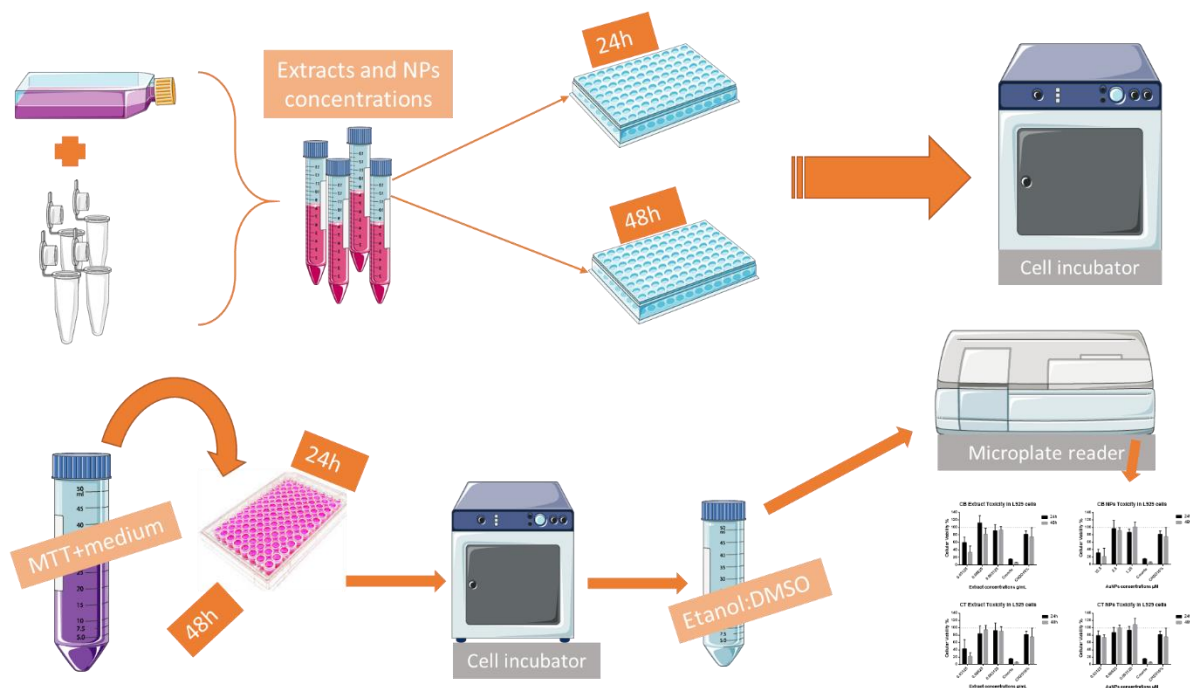
**Figure 8**-Schematic summary of MTT assay.

2.2.2 Wound-healing assay

Cell migration and proliferation were assessed through the **wound-healing assay,** which evaluates the migration capacity of the cells. It was done a scratch in each well at the bottom surface already seeded with BJ-5ta or L 929 cells. Cell migration was observed in the IX71 Inverted Fluorescent Microscope (Olympus), and the results were recorded in photographs at different time points. The free area of the photos was measured with Image J and then converted to percentage in relation to the area devoid of cells at 0 h. If the wells with the tested systems have better performance than the control (cells incubated only with culture medium) it means the system have regeneration properties.

Extract solutions of *CB* and *CT* and derived NPs were prepared by dilution of respective stock solutions in the appropriate culture medium for cells, in order to obtain the nominal test concentrations: 0.03125 g/mL, 0.00625 g/mL and 0.003125 g/mL for extracts, and 12.5 µM, 2.5 µM and 1.25 µM for NPs.

Cells were seeded into 12 well-microplates in 1 mL of culture medium at a cell density of 2×10^5 (for BJ-5ta) and 8×10^4 (for L929) cells/well, and incubated for 24h, at 5 % CO_2 and 37 ˚C an incubator (C150 – Binder).

This assay was performed following in two different strategies: at the first, the cells were incubated with the extracts and NPs and then the scratch of the confluent cell culture was performed (to see if there was any protective property). For that, the culture medium of adhered cells was removed and 1 mL of the different nominal concentrations of extracts and NPs were added to the wells, in duplicates. After 10 h, the scratch was performed and the results were recorded in photographs at 0, 10, 18 and 22 h. In the

second strategy, first a scratch was performed and then the cells were incubated with the extracts and the NPs (to see if there was any regeneration property). For that, the culture medium of adhered cells was removed, the scratch was performed and 1 mL of the different nominal concentrations of extracts and NPs were added to the wells, in duplicates. Same time points were established. A negative control was performed for comparison with tested conditions (cell incubation with culture medium). Cells were maintained in an incubator with 5 % CO_2, at 37 ˚C for 24 h (**Figure 9**).
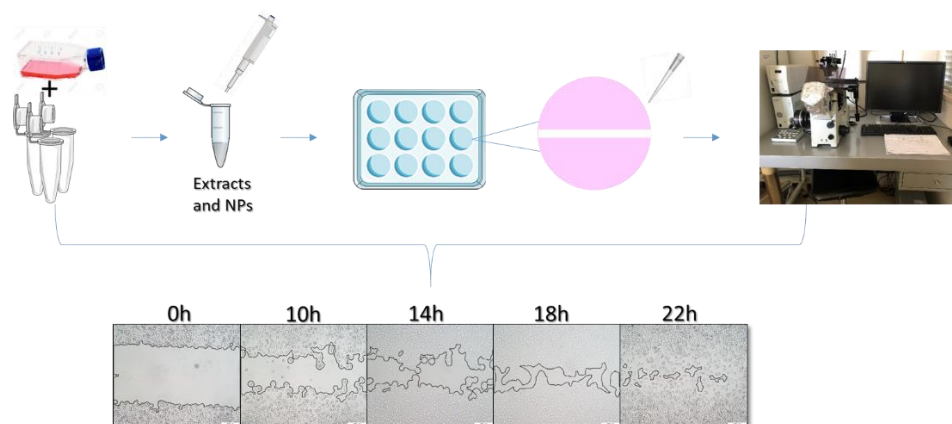
Figure 9-Wound-Healing assay protocol scheme.

2.3 *In vivo* Assay

2.3.1   Zebrafish Embryo toxicity Test (ZET)

A study[25] showed that *in vitro* vs. *in vivo* toxicity correlation, as well as the elucidation of potential discrepancies, has important implications for facilitating the translation of nanomedicine materials into clinical trials. *In vivo*, zebrafish-mediated experiments can serve as an intermediate step between cell-based and mammalian testing, thus streamlining the drug development time-line[40]. In this protocol, first, viable eggs are incubated with the test compounds up to 2 h_{pf}, maximizing uptake by the embryo's chorion. Then, observations are made at 8, 32, 56 and 80 h_{pf}. Finally, several parameters are evaluated as, mortality, epibolic arc, heartbeat and others. In this work, *in vivo* toxicity of each nanocarrier and related constituents was assessed via ZET Assay.

Hence, mature zebrafish specimens were isolated and used to produce the embryos. Next day, these returned to the stock aquarium and eggs were collected. After, these, were cleared and death and non-fertilized eggs were identified (not to be selected), by direct observation. 10 viable embryos were then placed per well, into 24-well microplates.

Extract solutions were prepared by dilution of the respective stock in HEPES, in order to obtain the test nominal concentrations defined (0.125 g/mL, 0.0625 g/mL, 0.03125 g/mL, 0.0125 g/mL, 0.00625

g/mL and 0.003125 g/mL).

Nanoparticles solutions were prepared by dilution of 0.4 mM stock in HEPES, in order to obtain the test nominal concentrations defined (12.5 µM, 5 µM, 2.5 µM and 1.25 µM).

Parameters observed in at each h, at microscope, are listed at **Figure 10**.

Figure 10 - Schematized figure of each hour and respective parameters.

All reagents used in the experiments are in **Table A** of Annexes.

III. RESULTS AND DISCUSSION

1. Characterization

In nanoparticles synthesis, the colour change observed and the appearance of the characteristic surface resonance band (SPR) of gold nanoparticles at 500 nm (Figure 13) allowed confirming their reduction and formation (**Figure 11**).

Figure 11- Brief scheme of the NPs synthesis and related UV-vis spectra.

Through the analysis of CTAu4 UV–Vis spectra (**Figure 12**), the characteristic surface plasmon resonance (SPR) absorption band of gold nanoparticles is at 537 nm.
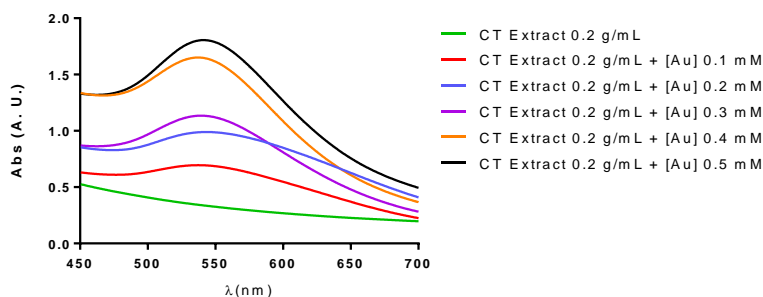
Figure 12- UV-vis spectra of the various concentrations of Au@CT, including CTAu4.

The reaction time was measured every 10 s for 2 h until the stabilization of the absorbance line, which takes 10 to 15 min, thus confirming the reduction and formation of nanoparticles (**Figure 13**).
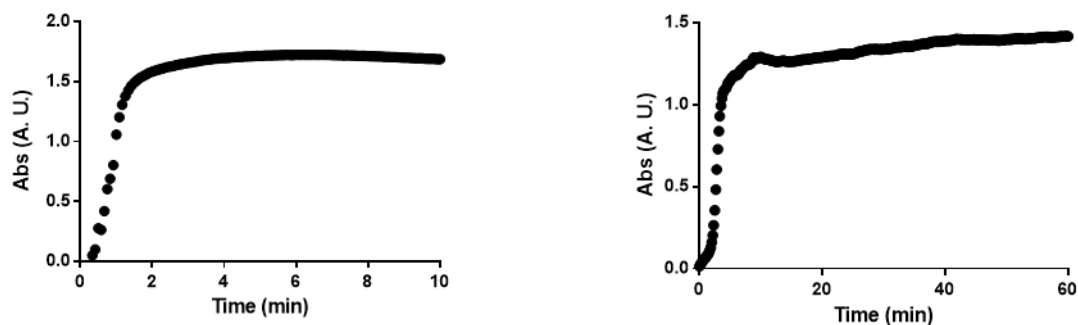
Figure 13- Time evolution of the intensity of the SPR band during the reaction of Au@CB (on the right) and Au@CT (on the left.

As it can be observed in **Figure 13**, the CB reaction time (< 15min) is faster than CT (15min).

For the purpose of assessing the stability of the NPs, the electrical potential was measured for Au@CB and Au@CT, -30.7±2.0 mV and -24.6±1.5 mV, respectively. These values indicate that Au@CB are highly stable and Au@CT are moderately stable.

The antioxidant activity of the extracts were evaluated by the determination of the reducing activity, total amount of phenolic compounds and DPPH scavenging activity as shown in **Table 2**. These assays were performed in order to analyse the potential of the extract to act as a reducing agent in the synthesis of nanoparticles. These parameters were also evaluated for NPs so that values among these could be compared and verified if the extracts were involved in their synthesis.

Table 2- Total phenolic content, reducing and DPPH scavenging activity of the extracts and Au@CT.

|	CB[30]	Au@CB[30]	CT	Au@CT
TPC (mg gallic acid/g algae)	2.41±0.09	2.47±0.21	9.26±0.34	6.15±0.21
Reducing Activity (mg ascorbic acid/g algae)	583.1±17.1	352.3±15.2	1783.6±60.2	1344.2±60.7
DPPH scavenging activity (EC50 mg/mL)	12.7±0.2	30.2±0.8	3.66±0.02	3.13±0.11

CT extract presented a strong antioxidant activity, once every values of the evaluated parameters were very high. When comparing these results with the ones obtained for *C. baccata* extract it can be observed that CT extract possess 10 times more reducing power, total phenolic content and a lower value of EC50.

However, the values of total phenolic content (TPC) and reducing activity obtained for Au@CT were lower, indicating that part of the phenols and other reductants presented in the extract were probably spent in the reducing process of nanoparticles synthesis.

Transmission Electron Microscopy (TEM) images were obtained for a better characterization. Nanoparticles showed a darker colour than the *Cystoseira tamariscifolia (CT)* extract. Nanoparticles were imbibed in the *CT* extract matrix, that acted as reducing and stabilizing agent.

Two of the nanoparticles made from *CT* extract (Au@CT), named CTAu4 and CTAu9, were particularly analysed as these were among those with the better narrow size range and significant monodispersity. Size distribution histograms were calculated from TEM images, assuming a spherical shape both for the free and embedded nanoparticles. Average particle size was 7.6 ± 2.2 nm and 14 ± 7.6 nm for CTAu4 and CTAu9, respectively.

As it can be seen at **Figure 14** and from the obtained data, CTAu4 showed the most ideal features, since NPs presented homogeneous size and shape.
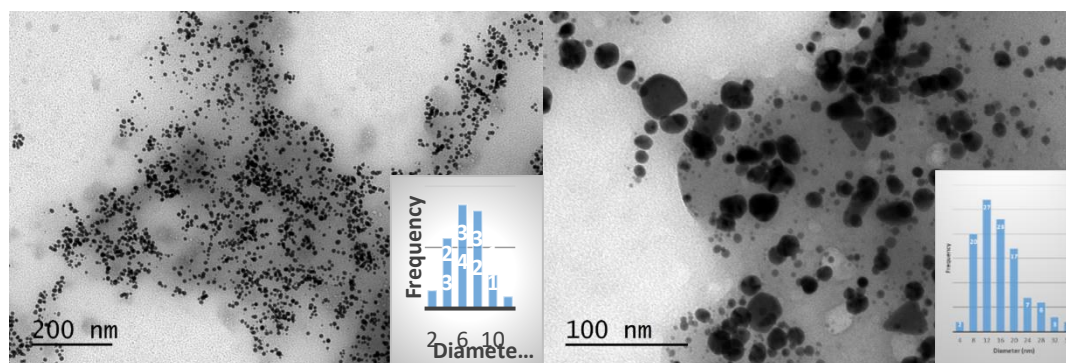
**Figure 14-**Low-magnification TEM images showing the obtained gold nanoparticles and some residual extract settled on the carbon film. Inset: size histogram of the particles using data obtained from TEM images (CTAu4 and CTAu9, respectively).

TEM analysis showed that the nanoparticles synthesized are spherical in both cases with diameters 7.6nm ± 2.2 nm for Au@CT and 8.4 nm ± 2.2 nm for Au@CB (**Figure 15**).
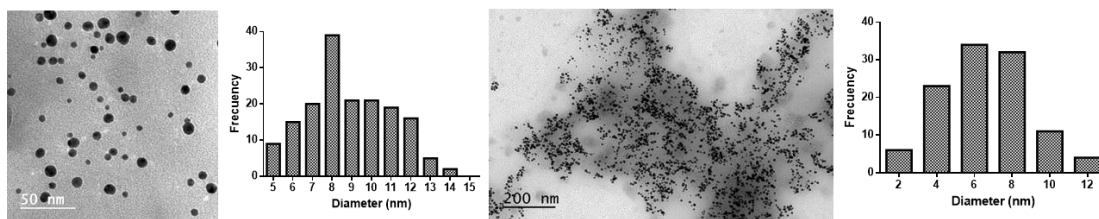
Figure 15- TEM images and their respective histogram of Au@CB (on the right) and Au@CT (on the left).

Fourier-Transform Infrared Spectroscopy (FTIR) spectral analysis (**Figure 16**) was carried out to identify the nature of the biomolecules involved in the synthesis of the nanoparticles (NPs). The assignation of the main bands was made based on previous reports and are collected in **Table 3**[30].
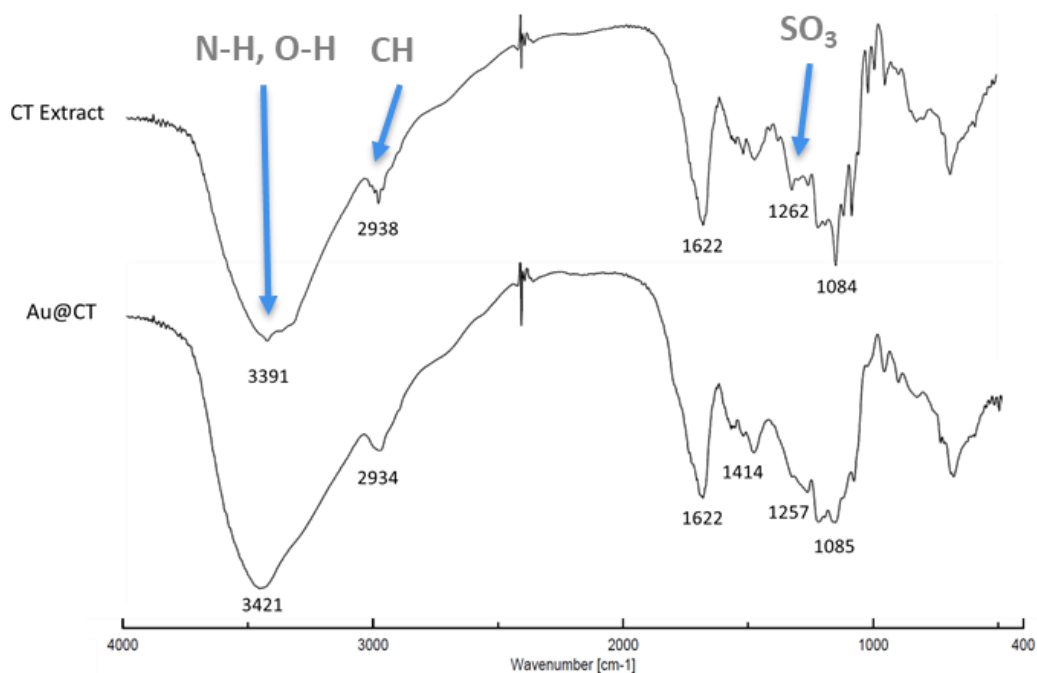
Figure 16- FTIR analyses spectra of CT and Au@CT with the functional groups that showed more differences.

Table 3-Band assignment (cm-1) for FTIR spectra obtained for CT and CB extracts and their respective NPs.

	C. baccata[30]	Au@CB[30]	C. tamariscifolia	Au@CT
ν N-H, O-H	3402	3284	3391	3421
ν (CH)	2937	2925	2938	2934
ν_{as}(CO)	1662	1627	1622	1622
ν_s (CO)	1417	1463	1413	1414
ν (SO$_3$)	1254	1261	1262	1257
ν (C-OH)	1078	1023	1084	1085

The strong broad band that appeared in both spectra between 3400 and 3300 cm^{-1} is assigned to NH stretching vibrations and OH stretching vibrations of the hydroxyl group of sugar, resulting from intermolecular and intramolecular hydrogen bonding[42]. The weak band at 2930 cm^{-1} can be assigned to aliphatic C-H groups stretching vibrations. The two broad bands at around 1600 and 1400 cm^{-1} are typically assigned to asymmetrical and symmetrical stretching of the carboxylate groups from amide I and II of proteins[43]. Bands between 1200 and 900 cm^{-1} are mainly due to C-C and C-O stretching bonds and glycosidic C-O-C vibrations, common to all polysaccharides[44].The signals at 1080 cm^{-1} can be attributed to the sugar ring and glycosidic bond C-O stretching vibrations[45,46]. The appearance of C-O-S bending vibration at 800 cm-1 and S-O stretching vibration at 1250 cm^{-1} attributed to sulphate esters indicates the presence of sulphate groups in the polysaccharide structure[47].

The shifts observed in the main bands suggests that the hydroxyl functional groups from polyphenols and polysaccharides or the amino groups of proteins might be involved in the bioreduction of the metals employed. Also, the carboxyl group from proteins has a strong ability to bind to metals so they could most possibly cap Au@NPs to prevent the agglomeration. In the same way, sulfonic groups from polysaccharides could be involved in metal binding.

2. *In vitro* Toxicity (MTT)
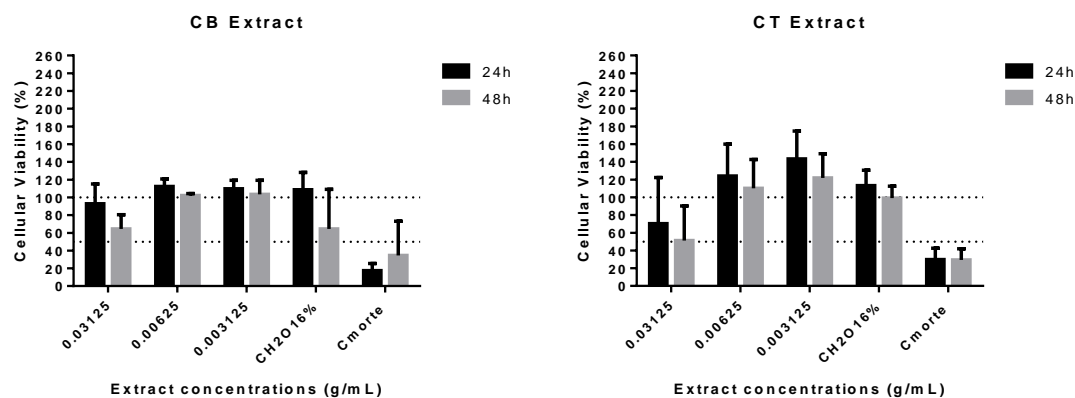
2.1 BJ-5ta cells

2.1.1 First trial

In order to define the best concentration range, a first trial was performed. The data collected (**Figure 17**) indicate that in these cells, metabolic activity is affected above 31.25 mg/mL of extract or 5 µM of gold nanoparticles (Au@CB). Therefore, three concentrations showing differences between viability and mortality were chosen: 0.003125, 0.00625 and 0.003125 g/mL for extracts and 12.5, 2.5 and 1.25 µM for NPs. These nominal concentrations were used at the following MTT and ZET assays.
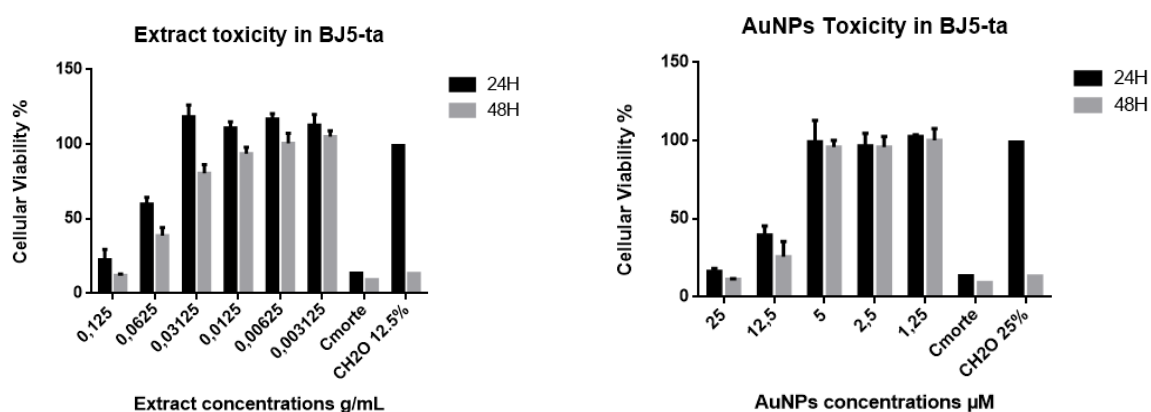
Figure 17-Cystoseira baccata extract and gold nanoparticles toxicity in normal fibroblasts (BJ5-ta) measured by MTT assay. The results are the mean ± standard deviation of independent experiments.

2.1.2 CB and CT extracts

Although some toxicity is noted at the highest concentrations for both algae extracts, these remain above 50 % of cellular viability (**Figure 18**). The highest concentration of CT extract induced more cytotoxicity than the highest concentration of CB extract. However, the other two lower concentrations seemed to cause a better response in CT extract since these remain above 100 % viability at 24 and 48 h.


38

In case of NPs, Au@CB only caused toxicity at the highest concentration, but Au@CT seems to correlate to a good percentage of viability at every test concentration (**Figure 19**).

In Au@CT, the percentage of cellular viability influenced by the two lower concentrations increased from 24 to 48 h of incubation, which could translate a higher cell proliferation in the presence the NPs.

2.1.3 Au@CB and Au@CT
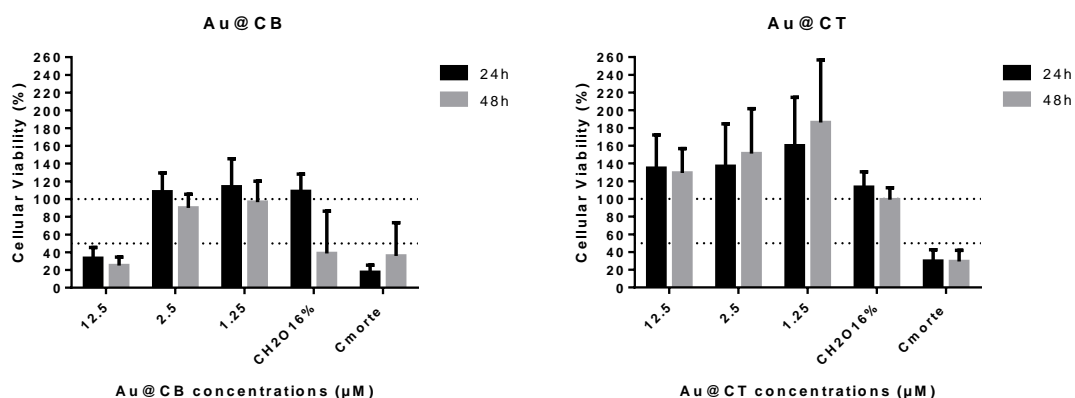
Figure 19-MTT data of AU@CB and Au@CT in BJ5-ta cells.

2.2 L 929 cells

2.2.1 CB and CT extracts

The extracts only induced toxicity at the highest concentrations, being more pronounced for CT extract (**Figure 20**). The lower concentrations caused a higher percentage of viability, but under than 100 %, except for CB extract, that at concentration of 0.00625 g/mL (24 h) caused a viability above that value.
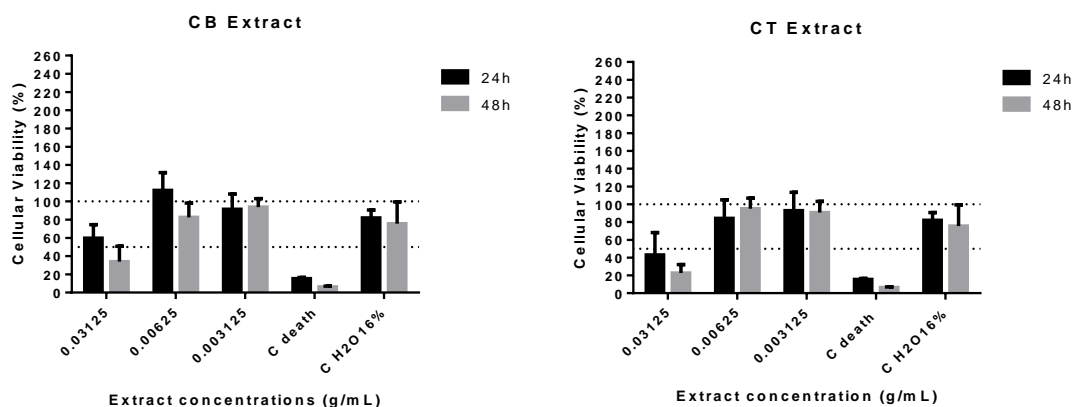
Figure 20- MTT data of CB and CT extracts in L929 cells.

2.2.2 Au@CB and Au@CT

Once again, Au@CT showed no cytotoxicity but Au@CB seems to be toxic at the highest concentration (causing viability under 50 %). For the lower concentration of *CB* extract and in the two low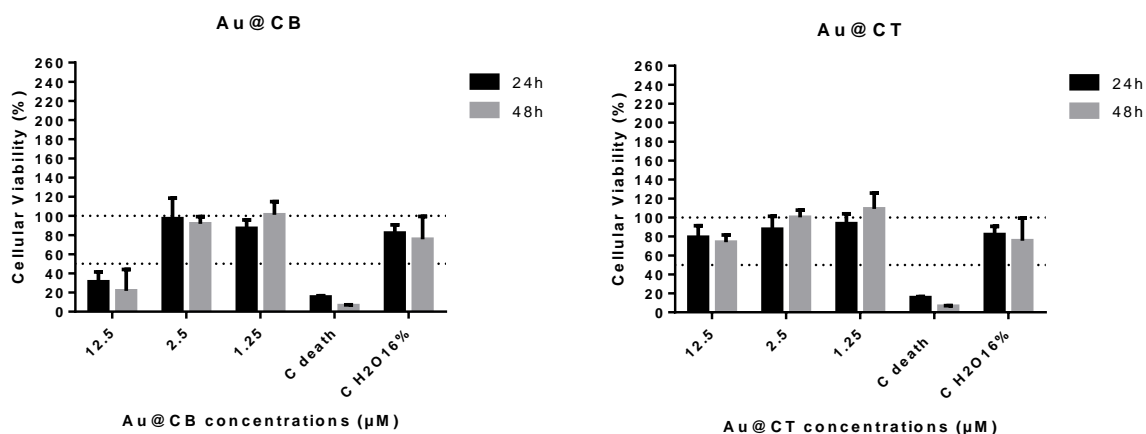er concentrations of *CT* extract, the percentage of viability in the cells increased from 24 to 48 h, showing again that NPs altered their proliferation, towards a higher percentage of viability (**Figure 21**).

Figure 21-MTT data of Au@CB and Au@CT in L929 cells.

Considering biomedical use as goal, toxicity testing should be addressed in tumour cells to evaluate biocompability and "targeted" cytotoxicity. In case of toxicity, it should be performed experiments to understand the mechanisms of specific cancer cells, using flow cytometry techniques.

In order to correlate these *in vitro* experiments with an *in vivo* model, the ZET assay was further performed. All the statistical data is available in Annexes (**Table B, C, D** and **E** for BJ-5ta cells and **Table F, G, H** and **I** for L929 cells).

3. *In vivo* Toxicity (ZET Assay)

3.1 CB and CT extracts

As it can be seen in **Figure 22**, only the highest concentration of *CT* extract affected zebrafish embryos, leading to lethal effects. The two lower concentrations caused a percentage of viability above 80 %, where the lowest concentration was better than control. Regarding *CB* extract, the highest concentration caused more than 60 % of viability, and the remaining concentrations induced a percentage of viability above 80 %.
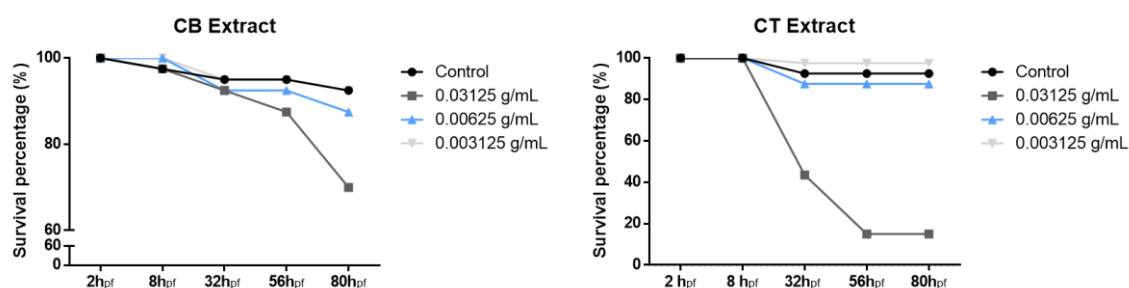
Figure 22-Survival data of zebrafish embryos exposed to CB and CT extracts for 80 h$_{pf}$.

3.1.1 Au@CB and Au@CT

In **Figure 23** it can be observed that Au@CT induced a higher viability percentage compared to Au@CB. All concentrations were above 80 % and the lower tested concentration even showed to be safer than the control. Au@CB also induced higher viability at the lower tested concentration when comparing with control. However, at the highest tested concentration, at 80 h$_{pf}$, the viability was reduced to 60 %.
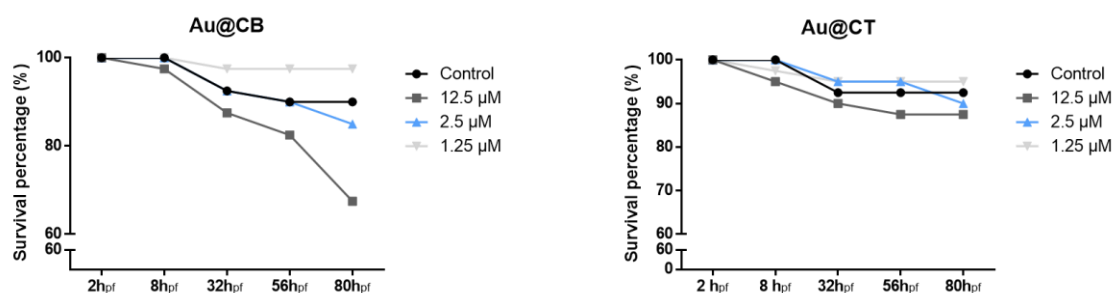
Figure 23-Survival data of zebrafish embryos exposed to Au@CB and Au@CT for 80 h$_{pf}$.

In vivo toxicity using the ZET assay indicates the same tendency as for cytotoxicity (**Table 4**).

Table 4-Lethal and sub-lethal effects of algae extracts and derived NPs in zebrafish embryos. (+) corresponds to a significant effect and (−) corresponds to a non-statistically significant effect on tested independent variables.

Parameters	Significant differences			
	CB extract	Au@CB	CT Extract	Au@CT
Cumulative survival (80 h_{pf})	-	+	+	-
Spontaneous movements (32 h_{pf})	+	+	+	-
Heart rate (32 h_{pf})	+	-	+	+
Heart rate (56 h_{pf})	+	+	-	+
Hatching (56h_{pf})	+	+	-	-
Free-swimming (80 h_{pf})	+	+	-	-
Epiboly (8h_{pf})	-	+	+	+
Head-trunk angle (32 h_{pf})	-	-	-	+
Pupil surface (co-variance: egg volume) (32 h_{pf})	–	+	-	-
Yolk volume (co-variance: egg volume) (32 h_{pf})	+	+	+	-
Yolk extension (co-variance: LT) (56 h_{pf})	-	-	-	-
L_T (56 h_{pf})	+	+	-	-

In general, regarding *CB*, the concentrations of extracts tested showed no lethal toxicity, but from the concentration 5 µM, lethal effects were recorded for NMs at the end of embryonic development. There

are no generally statistically relevant differences between the extracts or NPs concentrations for the epiboly and head-trunk angle parameters so, developmental delays must have occurred between 8 and 32 h_{pf}, and recorded mainly from 0.03125 g/mL (for extracts) and 12.5 µM (for NPs) concentrations. Statistically relevant differences in hatching rates of extracts or NPs are relatively erratic but the significant decrease in spontaneous movements may correlate, reflecting an effect on the primitive spinal network, which acts as their activation substrate. A statistically significant decrease in heart rate and free-swimming of extracts or NPs reflects an effect at the level of secondary neuromotor circuits, at a more mature stage of development, which act as their activation substrate, namely at the level of the rhombencephalon conserved among vertebrates. There are indications of traffic effects and lipid metabolism that should be discussed more effectively after confirming the errors detected in the data, and statistically relevant differences were recognized for yolk volume, pupil surface, yolk extension and L_T for extracts and NPs, seeming to point to a ''lipophilic affinity'' entrapment effect, in the early developmental, at the yolk level, with embryos having increased yolk volumes and decreased pupils and body size at later stages of development.

In the case of *CT*, extract concentrations caused lethality above all at the highest tested concentration corresponding to 0.03125 g/mL; lethal effects were not recorded for NPs. There are generally statistically relevant differences between extract concentrations or NPs for the epiboly and head-trunk angle parameters, which appear to reflect a concentration-dependent negative feedback effect, in which initial developmental delays during gastrulation tend to be compensated at later stages, notably during the pharyngeal, leading even at the highest concentrations to an accelerating tendency of extract development and a statistically relevant effect for NPs. Although a concentration-dependent decrease (significant for extracts, tendency towards NPs) is observed in spontaneous movements, it does not significantly affect the hatching rate. Lower concentrations of NPs appear to reflect an effect on the spinal network which acts as their activation substrate rather than the maximal concentration tested, which appears to ''protect'' in the sense that it conserves the normal embryo development, similar to the control group - the same pattern holds for yolk volume (in NPs) - a traffic imbalance and lipid metabolism caused by these lower concentrations of NPs may be due to the fact that they are more likely to cross the protein channels of the chorion, probably due to a lower tendency to form clusters, and therefore tend to maintain their nanosize. A statistically significant decrease in heart rate of extracts or NPs does not appear to be due to an effect on secondary neuromotor circuits, as there are no statistically relevant differences in free-swimming that occurs similarly at a more mature stage of development. There are indications of effects on trafficking and lipid metabolism that should be discussed more effectively after confirming the errors

detected in the data, and statistically relevant differences were generally recognized for eye and yolk volume and eye surface but not pupil, yolk extension or L_T for extracts and NPs, seeming to point (taking into account the data collected as a whole) rather to a "localized", eventually gene-mediated effect - OBs: it has been shown that the breakdown of specific genes that instruct the zebrafish lipid homeostasis regulatory network impairs lipid deposition, supporting the role of these genetic sensors in the normal development of the central nervous system, so a possible change in their expression levels as a consequence of exposure to extracts or NPs is a rational assumption that must be neglected; so instead of equating an effect on lipid transfer rate from the deposition points to the organism, a possible interference in the expression patterns of the genes that govern lipid accumulation in the affected target sites could support the reported result.

In another work that studied the Au@NPs toxicity in the zebrafish embryos, the results presented low toxicity to the early stages of zebrafish development[48], being in conformity with the obtained results.

After toxicity tests, it was decided to study cell migration and proliferation in presence of these extracts and nanoparticles since taking into account cytotoxicity data, in some cases, it seemed that there was an improvement in viability from 24 to 48 h.

All the statistical data is in Annexes (**Figure a** to **n**).

4. *In vivo* cell migration (Wound-Healing Assay)

This assay was performed in two different strategies, pre and post-incubation. For both cases, the free percentage area when in presence of the systems was compared to the control, to determine if the scratch closure was faster or slower than at the control.

In pre-incubation approach, first it was made a 12 h incubation with the extracts and NPs and just then the scratch, to evaluate their effects at a long term in the cells. In post-incubation test, first it was made the scratch and immediately the cells were incubated with the extracts and NPs, therefore to evaluate the immediate interaction between these and the cells.
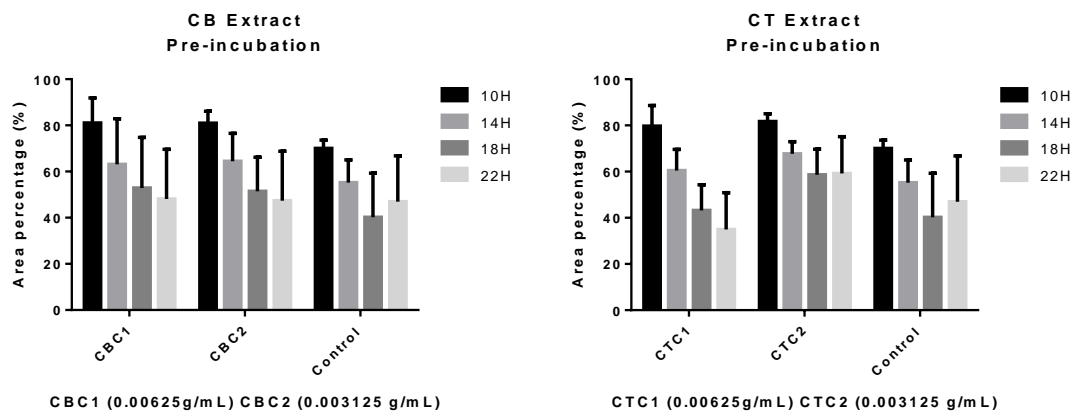
4.1 BJ-5ta cells

4.1.1 Pre-incubation

a. CB and CT extracts

With CBC1, CBC2 and CTC2 incubation conditions, the area percentage of the scratch was larger than that observed in the control, showing that these conditions do not cause any protective effect (**Figure 24**). CTC1 started to cause effect at 22 h, however it has to be taken into account the cell line doubling time, which is around 24 h, so results could not reflect the "help effect" in cell migration and proliferation

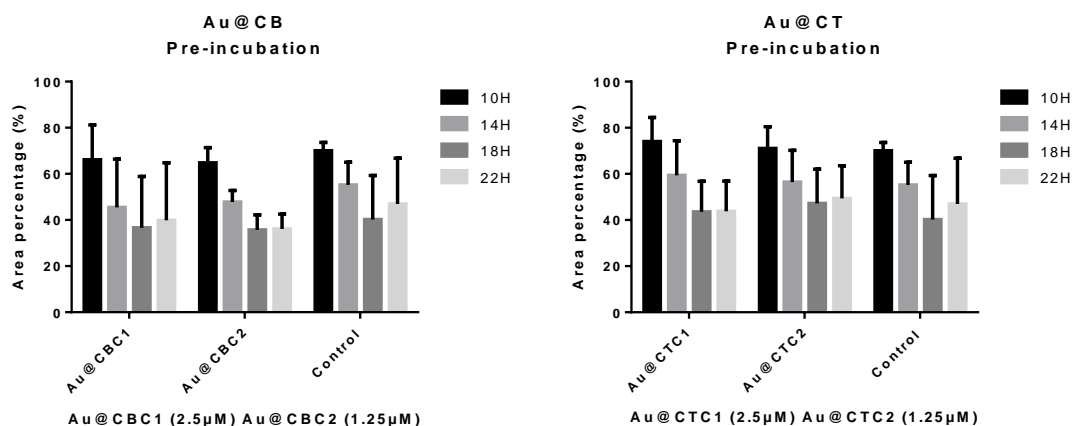caused by the extract but rather a natural cell doubling effect.

Figure 24- Wound-healing assay data for pre-incubation of CB and CT extracts in BJ-5ta cells.

b. Au@CB and Au@CT

Au@CB concentrations presented very similar results to control after 10 h, but in the following hours, for both test concentrations, these influenced the migration and proliferation of the cells so there was less area percentage than that of the control group, which indicates that these started an effect (**Figure 25**). Au@CT concentrations were equal to control, but relatively worst, so these did not have an effect.
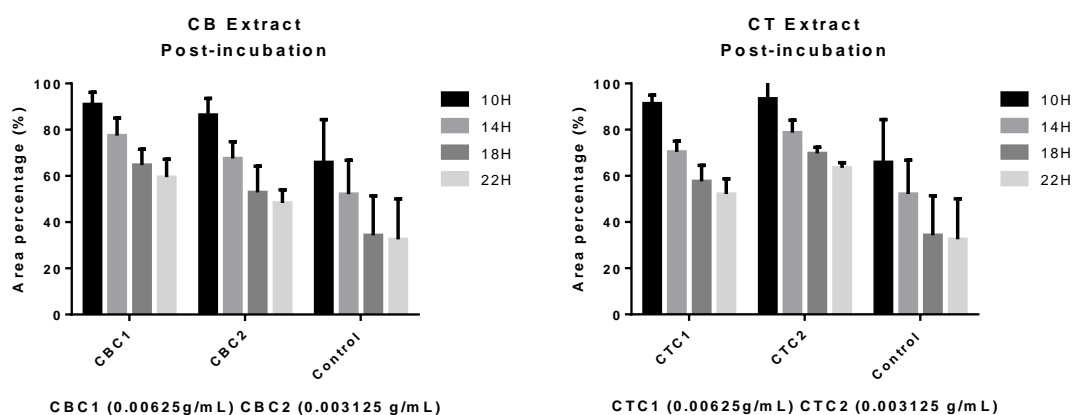

Figure 25-Wound-healing assay data for pre-incubation of Au@CB and Au@CT in BJ-ta cells.

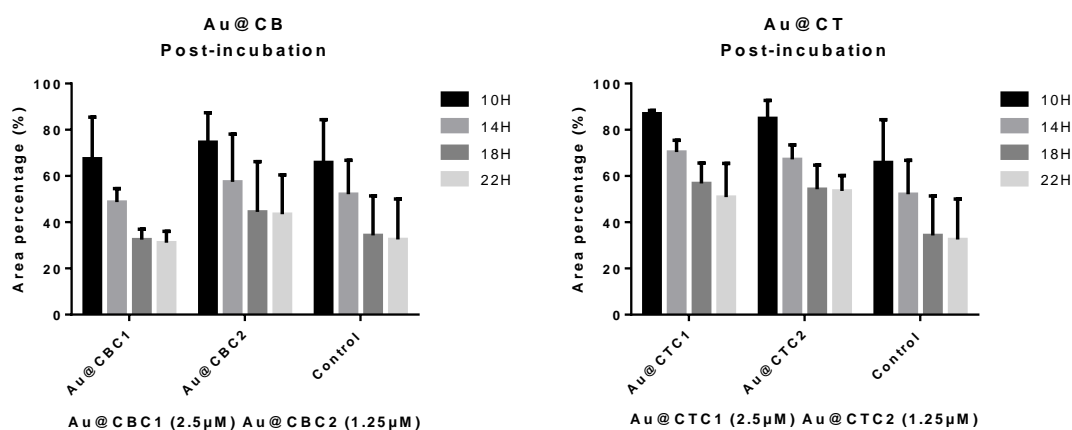### 4.1.2 Post-incubation
a. CB and CT extracts

The area percentage of the two extracts were worse than control, indicating that these have no regenerative effect (**Figure 26**).

Figure 26-Wound-healing assay data for post-incubation of CB and CT extracts in BJ-5ta cells.

b. Au@CB and Au@CT

Cells influenced by Au@CB and Au@CT showed a minor percentage area than control. In conclusion, there is no effect from both nanoparticles (**Figure 27**).
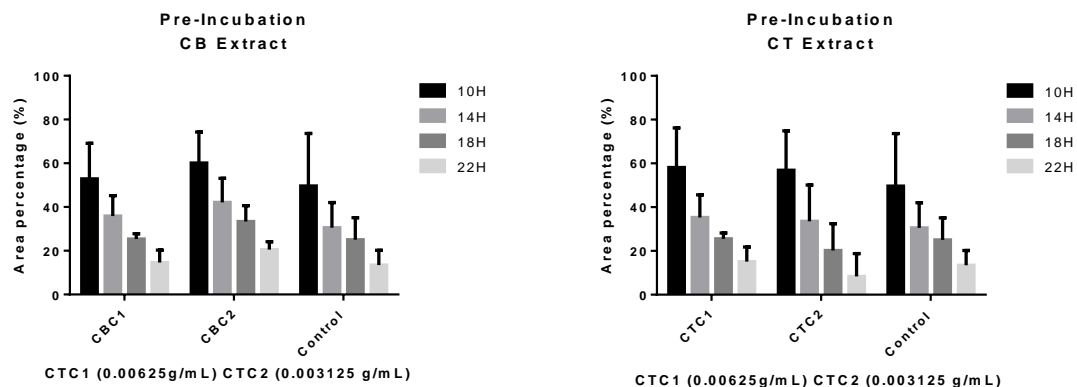

Figure 27-Wound-healing assay data for post-incubation of Au@CB and Au@CT in BJ-5ta cells.

4.2 L 929 cells

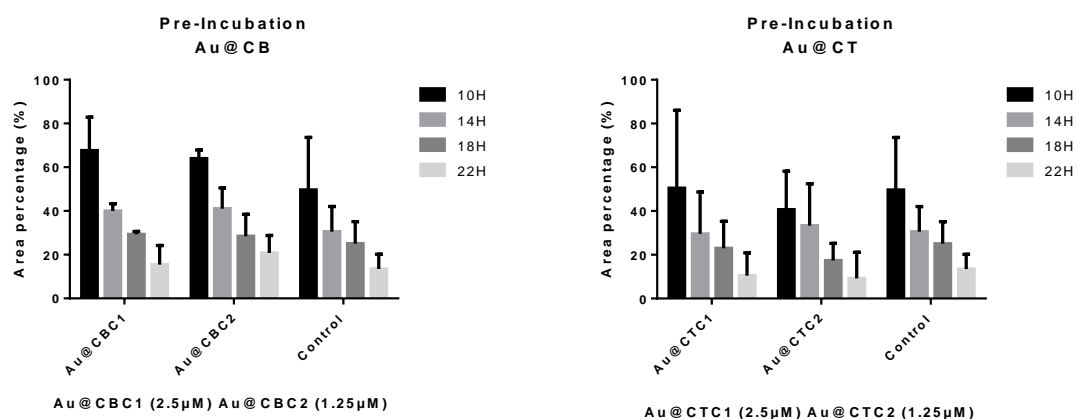#### 4.2.1 Pre-incubation

a. CB and CT extracts

CB extract concentrations showed no protective properties on cells. From CT extract, only CTC2 induced an effect after 18 h (**Figure 28**). This happened probably because of the extra time that cells had in pre-incubation with the extracts and nanoparticles, where these could start "losing" their properties and thus causing less stress on cells.

Figure 28-Wound-healing assay data for pre-incubation of CB and CT extracts in L 929 cells.

b. Au@CB and Au@CT

None Au@CB test concentrations caused an effect on cells. Both Au@CT concentrations started to induce an effect just after 10 h, being more pronounced for Au@CTC2 (**Figure 29**).
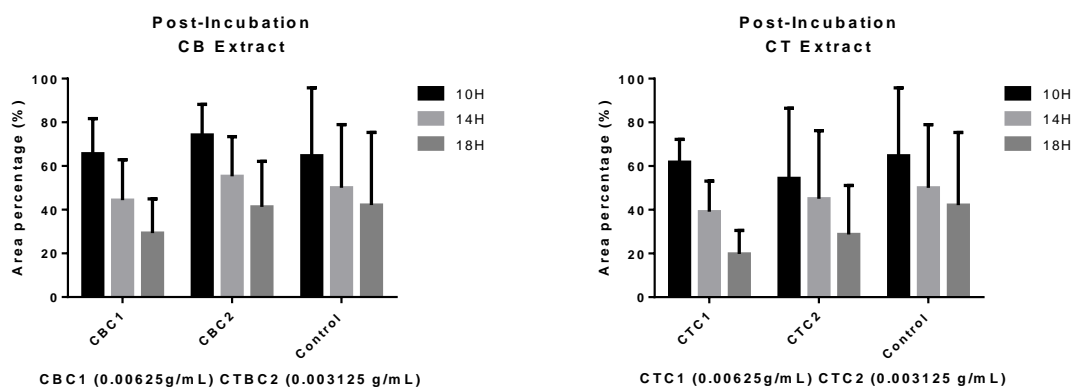

Figure 29-Wound-healing assay data for pre-incubation of Au@CB and Au@CT in L929 cells.

4.2.2 Post-incubation
a. CB and CT extracts

Cells proliferation and migration induced by CBC1, CTC1 and CTC2 were more pronounced than that registered at the control group, starting from 14 h, indicating that these might have regenerative effects. CBC2 did not exert effect (**Figure 30**).
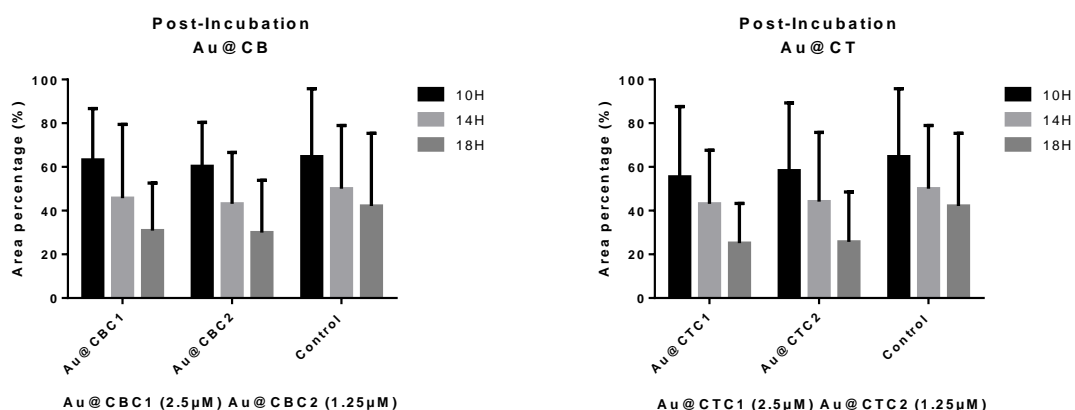
Figure 30-Wound-healing assay data for post-incubation CB and CT extracts in L 929 cells.

b. Au@CB and Au@CT

Au@CB concentrations started to cause an effect after 14 h, while Au@CT induced an earlier effect, after 10 h (**Figure 31**).

Figure 31-Wound-healing assay data for post-incubation of Au@CB and Au@CT in L929 cells.

In BJ-5ta cell line and considering pre-incubation trial, both extracts and NPs did not induced an effect. In post-incubation, only CTC1 (after 18 h), and at both concentrations of Au@CB (after 10 h) exerted an effect. In L 929 cell line and considering a pre-incubation trial, both concentrations from *CT* and CBC2 started to cause an effect after 14 h. For NPs, both concentrations of Au@CB and Au@CT induced an effect, after 14 and 10 h, respectively. In post-incubation assay, only CTC2 (after 18 h) and at both concentrations of Au@CT (after 10 h) exerted an effect.

In this experiment, it was not evaluate the cellular migration and proliferation after 22 h because the results might not be correct for the first as it could be influenced by cell line doubling time.

All the statistical data is in Annexes (Table **J** and **K**).

L 929 cells were used in another work with a different algaes species, *Sargassum illicifolium*, and the results showed that cell proliferation and migration were significantly faster in those treated with aqueous extracts when compared with the control group. Moreover, no cytotoxic effect of aqueous extracts on L 929 cell line was observed. Therefore, the study suggested that these algae extracts might compose a potential therapeutic agent for skin wound healing by promoting fibroblast proliferation and migration. Also, it was underlined that further studies are highly warranted to identify active molecules in the extracts and in vivo studies would verify wound healing therapeutic applications shown there[49].

Here, *in vitro* wound-healing assay showed a good perspective of the possibly regeneration effects but, besides the need of more replications to consolidate the results, it is also critical to investigate a valid screening and evaluation tool, on *in vivo* models, for preclinical wound therapeutic development from liquid to (semi-)solid systems to improve the predictability[50].

Laminaran, a polysaccharide extracted from the brown seaweed *Cystoseira barbata* was used to investigate the effectiveness for healing full thickness wounds induced on rats. This study revealed an improved collagen deposition, and increased fibroblast and vascular densities composed a scientific *in vivo* evidence of the efficiency of the compound as a wound healing agent of interest in modern medicine[51]. Therefore, as the studied algae are from the same genus, hereafter it could be investigated if associated compounds can also be present on these and if have bioactivity, if show some kind of toxicity and how affects migration and proliferation in cells and other *in vivo* models.

IV. CONCLUSIONS

A simple, environmentally-friendly and low-cost-effective method was replicated for the efficient synthesis of colloidal AuNPs (gold nanoparticles) using, for the first time, an aqueous extract of the macroalgae *C. tamariscifolia*. The formation of spherical, stable nanoparticles was demonstrated by UV–vis spectroscopy, TEM and FTIR. However FTIR spectra analysis have been performed, the biomolecules involved in the synthesis need to be better elucidated. In this manner, the mechanisms that mediate the synthesis of this biological NPs should be studied in detail to identify these biomolecules and perhaps to also improve the properties of nanoparticles.

Cystoseira genus has a wide variety of compounds with interesting biological properties, it is important to lead more researches to find and study even more compounds with different biological activities, like antileishmanial activity. Also, it should be evaluate the biocompability and toxicity of them to make possible their use in clinical cases.

According to MTT and ZET assay, the extracts only induced toxicity at the highest concentrations tested, in cells and zebrafish embryos, being more pronounced for *CT* extract. In NPs (nanoparticles), (also in cells and zebrafish embryos) only the Au@CB (NPs from CB) caused toxicity in the highest concentration. The Au@CT (NPs from CT) did not present toxicity.

In wound-healing assay, in general, *CT* extract and Au@CT showed a more significant and earlier effect for pre and post-incubation, indicating these can exert more expressive regenerative and protective effects. Also, the NPs showed less toxicity in general compared to extracts. Having into account this assay, a previous experiment[52], on HaCaT (human keratinocytes cells), demonstrated that keratinocyte growth factor (KFG), a secreted protein cross-linked with the surface of AuNPs displayed a good colloidal stability, decent biocompability and insignificant cytotoxicity. It was proven that this breed had better experimental results promoting the migration and proliferation of the keratinocytes than the bare AuNPs. Furthermore, in animal full-thickness wound model, the linked system enhanced wound healing by promoting wound re-epithelialization rather than granulation. The superior biocompatibility, colloidal depressiveness and biological activity of this nanocomposite indicated that it could be utilized as a promising wound healing agent for clinical application in the future. Therefore, since our study targeted biomedical applications, in the hereafter this could be assessed on a compound presenting affinity to bound to the nanoparticles, that would improve the chemical bounds and potentially permit to compose a targeted nano delivery system towards enhanced wound-healing, and more controlled toxic effects.

In the future, after some studies about the complex interaction between the molecules and identification

of the functional groups involved in the synthesis of the NPs and the complex interactions between these and the cells, green synthesis could be a common and more standardized method to be used. Advantages from that are great, especially in a time where taking care of our planet is so important and the conscious acts about this issue can start on our laboratories.

Green synthesis of NPs, if in a few years really could result and the industrial production could be made with the help of genetic engineering, starting to create artificial algae with the interest properties.

V. REFERENCES

1. Silva, L. P. *et al.* Nanotecnologia verde para síntese de nanopartículas metálicas. *Biotecnol. Apl. à Agro&Indústria - Vol. 4* 967–1012 (2017).
2. Noah, N. *Green synthesis: Characterization and application of silver and gold nanoparticles. Green Synthesis, Characterization and Applications of Nanoparticles* (Elsevier Inc., 2019).
3. Nasrollahzadeh, M., Atarod, M., Sajjadi, M., Sajadi, S. M. & Issaabadi, Z. *Plant-Mediated Green Synthesis of Nanostructures: Mechanisms, Characterization, and Applications. Interface Science and Technology* **28**, (Elsevier Ltd., 2019).
4. Rai, M. Nanobiotecnologia verde: biossínteses de nanopartículas metálicas e suas aplicações como nanoantimicrobianos. *Cienc. Cult.* **65**, 44–48 (2013).
5. Iravani, S. Green synthesis of metal nanoparticles using plants. *Green Chem.* **13**, 2638–2650 (2011).
6. Khanna, P., Kaur, A. & Goyal, D. Algae-based metallic nanoparticles: Synthesis, characterization and applications. *J. Microbiol. Methods* **163**, 105656 (2019).
7. Mahdavi, M., Namvar, F., Ahmad, M. Bin & Mohamad, R. Green biosynthesis and characterization of magnetic iron oxide (Fe 3O4) nanoparticles using seaweed (Sargassum muticum) aqueous extract. *Molecules* **18**, 5954–5964 (2013).
8. Bruno de Sousa, C. *et al.* Cystoseira algae (Fucaceae): update on their chemical entities and biological activities. *Tetrahedron Asymmetry* **28**, 1486–1505 (2017).
9. de Sousa, C. B. *et al.* Improved phylogeny of brown algae Cystoseira (Fucales) from the Atlantic-Mediterranean region based on mitochondrial sequences. *PLoS One* **14**, 1–23 (2019).
10. Cabios'h J., Floc'h J. Y., Le Toquin A., Boudouresque C. F., Meinesz A., V. M. *Guía De Las Algas del Atlantico y del Mediterraneo*. (2007).
11. Otero Jorge, Comesaña Patricia, C. M. *Guia das Macroalgas de Galicia*. (2002).
12. Celis-Plá, P. S. M. *et al.* Seasonal biochemical and photophysiological responses in the intertidal macroalga cystoseira tamariscifolia (Ochrophyta). *Mar. Environ. Res.* **115**, 89–97 (2016).
13. The Royal Society *et al.* Nanoscience and nanotechnologies: opportunities and uncertainties. *London R. Soc. R. Acad. Eng. Rep.* **46**, 618–618 (2004).
14. Stephen J. Fonash, M. V. de V. *What, Why, and Why Now?* (Engineering, Medicine and Science at the Nano-Scale, 2018).
15. Farzin, L., Sheibani, S., Moassesi, M. E. & Shamsipur, M. An overview of nanoscale radionuclides and radiolabeled nanomaterials commonly used for nuclear molecular imaging and therapeutic functions. *J. Biomed. Mater. Res. - Part A* **107**, 251–285 (2019).
16. Heinz, H. *et al.* Nanoparticle decoration with surfactants: Molecular interactions, assembly, and applications. *Surf. Sci. Rep.* **72**, 1–58 (2017).
17. Singh, P., Kim, Y. J., Wang, C., Mathiyalagan, R. & Yang, D. C. The development of a green approach for the biosynthesis of silver and gold nanoparticles by using Panax ginseng root extract, and their biological applications. *Artif. Cells, Nanomedicine Biotechnol.* **44**, 1150–1157 (2016).
18. Majdalawieh, A., Kanan, M. C., El-Kadri, O. & Kanan, S. M. Recent Advances in Gold and Silver Nanoparticles: Synthesis and Applications. *J. Nanosci. Nanotechnol.* **14**, 4757–4780 (2014).
19. Rizvi, S. A. A. & Saleh, A. M. Applications of nanoparticle systems in drug delivery technology. *Saudi Pharm. J.* **26**, 64–70 (2018).
20. Din, F. U. *et al.* Effective use of nanocarriers as drug delivery systems for the treatment of selected tumors. *Int. J. Nanomedicine* **12**, 7291–7309 (2017).
21. Gatzka, M. V. Targeted tumor therapy remixed—an update on the use of small-molecule drugs in

combination therapies. *Cancers (Basel).* **10**, (2018).

22. Ventola, C. L. Progress in nanomedicine: Approved and investigational nanodrugs. *P T* **42**, 742–755 (2017).

23. Gwinn, M. R. & Vallyathan, V. Nanoparticles: Health effects - Pros and cons. *Environ. Health Perspect.* **114**, 1818–1825 (2006).

24. Jeevanandam, J., Barhoum, A., Chan, Y. S., Dufresne, A. & Danquah, M. K. Review on nanoparticles and nanostructured materials: History, sources, toxicity and regulations. *Beilstein J. Nanotechnol.* **9**, 1050–1074 (2018).

25. Seabra, A. & Durán, N. Nanotoxicology of Metal Oxide Nanoparticles. *Metals (Basel).* **5**, 934–975 (2015).

26. Bawani, K. Biology of zebrafish, Danio rerio. (2014).

27. Kimmel, C. B., Ballard, W. W., Kimmel, S. R., Ullmann, B. & Schilling, T. F. Stages of embryonic development of the zebrafish. *Dev. Dyn.* **203**, 253–310 (1995).

28. OECD. Test Guideline 203. Fish, Acute Toxicity Test. *OECD Guidel. Test. Chem.* 1–23 (2019).

29. Eimon, P. M. & Rubinstein, A. L. The use of in vivo zebrafish assays in drug toxicity screening . *Expert Opin. Drug Metab. Toxicol.* **5**, 393–401 (2009).

30. González-Ballesteros, N., Prado-López, S., Rodríguez-González, J. B., Lastra, M. & Rodríguez-Argüelles, M. C. Green synthesis of gold nanoparticles using brown algae Cystoseira baccata: Its activity in colon cancer cells. *Colloids Surfaces B Biointerfaces* **153**, 190–198 (2017).

31. Shalaby, E. A. Algae as promising organisms for environment and health. *Plant Signal. Behav.* **6**, 1338–1350 (2011).

32. Sharma, V. K., Yngard, R. A. & Lin, Y. Silver nanoparticles: green synthesis and their antimicrobial activities. *Adv. Colloid Interface Sci.* **145**, 83–96 (2009).

33. Freile-Pelegrín, Y. & Robledo, D. Bioactive Phenolic Compounds from Algae. *Bioact. Compd. from Mar. Foods Plant Anim. Sources* 113–129 (2013).

34. Vizetto-Duarte, C. *et al.* Can macroalgae provide promising anti-tumoral compounds? A closer look at Cystoseira tamariscifolia as a source for antioxidant and anti-hepatocarcinoma compounds . *PeerJ* **4**, e1704 (2016).

35. Vizetto-Duarte, C. *et al.* Isololiolide, a carotenoid metabolite isolated from the brown alga Cystoseira tamariscifolia, is cytotoxic and able to induce apoptosis in hepatocarcinoma cells through caspase-3 activation, decreased Bcl-2 levels, increased p53 expression and PARP cleava. *Phytomedicine* **23**, 550–557 (2016).

36. Harris, D. C. *Quantitative Chemical Analysis*. (2008).

37. Zinin, P. Advanced Techniques in Geophysics and Materials Science Transmission Electron Microscope Resolution of SEM. *Univ. Hawaii* 1–43 (2010).

38. Bhattacharjee, S. DLS and zeta potential - What they are and what they are not? *J. Control. Release* **235**, 337–351 (2016).

39. González-Ballesteros, N., Rodríguez-González, J. B. & Rodríguez-Argüelles, M. C. Harnessing the wine dregs: An approach towards a more sustainable synthesis of gold and silver nanoparticles. *J. Photochem. Photobiol. B Biol.* **178**, 302–309 (2018).

40. Rizzo, L. Y., Golombek, S. K., Mertens, M. E. & Pan, Y. Europe PMC Funders Group In Vivo Nanotoxicity Testing using the Zebrafish Embryo Assay. *J Mater Chem B Mater Biol Med* 1–13 (2013).

41. Karumuri, B. Metabolic Assay Based Validation of Cell Viability to Inflammatory Stimuli and Anti-Cancer Drugs in Normal and Tumor Brain Glia (2016).

42. Rodrigues, D. *et al.* Chemical composition of red, brown and green macroalgae from Buarcos bay in Central West Coast of Portugal. *Food Chem.* **183**, 197–207 (2015).

43. Fernández, P. V., Ciancia, M. & Estevez, J. M. Cell wall variability in the green seaweed codium

vermilara (bryopsidales chlorophyta) from the argentine coast. *J. Phycol.* **47**, 802–810 (2011).

44. Estevez, J. M., Fernández, P. V., Kasulin, L., Dupree, P. & Estevez, J. M. Chemical and in situ characterization of macromolecular components of the cell walls from the green seaweed Codium fragile. *Glycobiology* **19**, 212–228 (2009).

45. Tabarsa, M., You, S. G., Dabaghian, E. H. & Surayot, U. Water-soluble polysaccharides from Ulva intestinalis: Molecular properties, structural elucidation and immunomodulatory activities. *J. Food Drug Anal.* **26**, 599–608 (2018).

46. El-Rafie, H. M., El-Rafie, M. H. & Zahran, M. K. Green synthesis of silver nanoparticles using polysaccharides extracted from marine macro algae. *Carbohydr. Polym.* **96**, 403–410 (2013).

47. Alipour, H. J., Rezaei, M., Shabanpour, B. & Tabarsa, M. Effects of sulfated polysaccharides from green alga Ulva intestinalis on physicochemical properties and microstructure of silver carp surimi. *Food Hydrocoll.* **74**, 87–96 (2018).

48. Pereira, A. C., Gomes, T., Ferreira Machado, M. R. & Rocha, T. L. The zebrafish embryotoxicity test (ZET) for nanotoxicity assessment: from morphological to molecular approach. *Environ. Pollut.* **252**, 1841–1853 (2019).

49. Premarathna, A. D. *et al.* Wound healing properties of aqueous extracts of Sargassum illicifolium: An in vitro assay. *Wound Med.* **24**, 1–7 (2019).

50. Planz, V., Wang, J. & Windbergs, M. Establishment of a cell-based wound healing assay for bio-relevant testing of wound therapeutics. *J. Pharmacol. Toxicol. Methods* **89**, 19–25 (2018).

51. Sellimi, S. *et al.* Antioxidant, antibacterial and in vivo wound healing properties of laminaran purified from Cystoseira barbata seaweed. *Int. J. Biol. Macromol.* **119**, 633–644 (2018).

52. Pan, A. *et al.* Topical Application of Keratinocyte Growth Factor Conjugated Gold Nanoparticles Accelerate Wound Healing. *Nanomedicine Nanotechnology, Biol. Med.* **14**, 1619–1628 (2018).

53. D'Costa, A. & Shepherd, I. T. Zebrafish Development and Genetics: Introducing Undergraduates to Developmental Biology and Genetics in a Large Introductory Laboratory Class. *Zebrafish* **6**, 169–177 (2009).

VI.   ANNEXES

A. Products and their respective companies and assays.

Company	Products	Reference	Assay
Analar Normapur	Ascorbic acid 99%	50-81-7	Reduction Power
	Gallic acid 99%	64-19-7	Fenolic Content
Biochrom	Fetal Bovine Serum (FBS)	S 0615	Subculturing
	Medium 199	FG 0615	Subculturing
	Trypsin	L2103	Subculturing
Carlo Erba Reagents	Etanol absolute anhydrous	308615	MTT
Fisher	Trichloroacetic acid 99%	76-03-9	AuNP synthesis
PanReac	Iron Chloride (III) 97%	15A813	Reduction Power
	Methanol 100%	131091	Reduction Power
	Potassium ferricyanide 98%	131505	DPPH
	Sodium Chloride	131659.1211	Subculturing
Scharlau	Sodium carbonate 99.5%	497-19-8	Fenolic Content
ATCC	BJ5-ta		MTT and wound-healing
ATCC	L929		MTT and wound-healing
Sigma-Aldrich	Antimycotic/antibiotic mix	A5955	Subculturing
	Dihydroxide sodium phosphate 99%	7601-54-9	Reduction Power
	Dimethyl sulfoxide (DMSO)	D8418	MTT
	Dulbecco's Modified Eagle's high glucose Medium (DMEM)	D-56-48	Subculturing
	Folin-Ciocalteu Reagent 2M Solution	47641	Fenolic Content
	Hygromycin	3274	Subculturing
	MTT (3-[4,5-dimethylthiazol-2-yl]-2,5-diphenyltetrazolium bromide)		MTT
	Potassium chloride (KCl)	P9541	Subculturing
	Sodium bicarbonate	S5761	Subculturing
	Sodium hydrogen phosphate Dodecahydrate ($Na_2HPO_4.12H_2O$)	71649	Subculturing
	Sodium Hidroxyde (NaOH)	S5881	pH adjustment
	Sodium hydroxide phosphate 99%	1310-73-2	Reduction Power
	Tetrachlorouric acid trihydrate 99.9%	16961-25-4	AuNP synthesis
	1,1-diphenyl-2-picryl-hydrazyl 97%	1707-75-1	DPPH

B. Statistic MTT data of CB extract in the BJ-5ta cells.

CB Extract (g/mL)	
0.03125 24h vs C_{death} 24h	*
0.00625 24h vs C_{death} 24h	**
0.00625 24h vs C_{death} 48h	*
0.00625 48h vs C_{death} 24h	**
0.00625 48h vs C_{death} 48h	*
0.003125 24h vs C_{death} 24h	**
0.003125 24h vs C_{death} 48h	*
0.003125 48h vs C_{death} 24h	**
0.003125 48h vs C_{death} 48h	*
CH_2O 16% 24h vs C_{death} 24h	**
CH_2O 16% 24h vs C_{death} 48h	*

C. Statistic MTT data of CB extract in the BJ-5ta cells.

CT Extract (g/mL)	
0.03125 48h vs 0.003125 24h	*
0.00625 24h vs C_{death} 24h	*
0.00625 24h vs C_{death} 48h	*
0.003125 24h vs C_{death} 24h	**
0.003125 24h vs C_{death} 48h	**
0.003125 48h vs C_{death} 24h	*
0.003125 48h vs C_{death} 48h	*

D. Statistic MTT data of Au@CB in the BJ-5ta cells.

Au@CB (µM)	
12.5 24h vs 1.25 24h	*
12.5 48h vs 2.5 24h	*
12.5 48h vs 1.25 24h	*
12.5 48h vs CH_2O 24h	*
2.5 24h vs C_{death} 24h	*
1.25 24h vs C_{death} 24h	**
CH_2O 24h vs C_{death} 24h	*

E. Statistic MTT data of Au@CT in the BJ-5ta cells.

Au@CT (µM)	
2.5 48h vs C_{death} 24h	*
2.5 48h vs C_{death} 48h	*
1.25 24h vs C_{death} 24h	*
1.25 24h vs C_{death} 48h	*
1.25 48h vs C_{death} 24h	**
1.25 48h vs C_{death} 48h	**

F. Statistic MTT data of CB extract in the L929 cells.

CB Extract (g/mL)	
0.03125 48h vs 0.00625 24h	**
0.03125 48h vs 0.003125 48h	*
0.00625 24h vs C_{death} 24h	***
0.00625 24h vs C_{death} 48h	***
0.00625 48h vs C_{death} 24h	*
0.00625 48h vs C_{death} 48h	**
0.003125 24h vs C_{death} 48h	*
0.003125 48h vs C_{death} 24h	**
0.003125 48h vs C_{death} 48h	***
C_{death} 24h vs CH_2O16% 24h	*
C_{death} 24h vs CH_2O16% 48h	*
C_{death} 48h vs CH_2O16% 24h	**
C_{death} 48h vs CH_2O16% 48h	**

G. Statistic MTT data of CT extract in the L929 cells.

CT Extract (g/mL)	
0.03125 24h vs 0.003125 48h	*
0.03125 48h vs 0.00625 24h	*
0.03125 48h vs 0.00625 48h	**
0.03125 48h vs 0.003125 24h	**
0.03125 48h vs 0.003125 48h	**
0.03125 48h vs CH_2O16% 24h	*
0.03125 48h vs CH_2O16% 48h	*
0.00625 24h vs C_{death} 24h	*
0.00625 24h vs C_{death} 48h	**
0.00625 48h vs C_{death} 24h	**
0.00625 48h vs C_{death} 48h	***
0.003125 24h vs C_{death} 24h	***
0.003125 24h vs C_{death} 48h	***
0.003125 48h vs C_{death} 24h	***
0.003125 48h vs C_{death} 48h	***
C_{death} 24h vs CH_2O16% 24h	**
C_{death} 24h vs CH_2O16% 48h	**
C_{death} 48h vs CH_2O16% 24h	***
C_{death} 48h vs CH_2O16% 48h	**

H. Statistic MTT data of Au@CB in the L929 cells.

Au@CB (μM)	
12.5 24h vs 2.5 24h	**
12.5 24h vs 2.5 48h	*
12.5 24h vs 1.25 24h	*
12.5 24h vs 12.5 48h	**
12.5 48h vs 2.5 24h	***
12.5 48h vs 2.5 48h	***
12.5 48h vs 1.25 24h	**
12.5 48h vs 1.25 48h	***
12.5 48h vs CH_2O16% 24h	**
12.5 48h vs CH_2O16% 48h	*
2.5 24h vs C_{death} 24h	****
2.5 24h vs C_{death} 48h	****
2.5 48h vs C_{death} 24h	***
2.5 48h vs C_{death} 48h	****
1.25 24h vs C_{death} 24h	***
1.25 24h vs C_{death} 48h	****
1.25 48h vs C_{death} 24h	****
1.25 48h vs C_{death} 48h	****
C_{death} 24h vs CH_2O16% 24h	**
C_{death} 24h vs CH_2O16% 48h	**
C_{death} 48h vs CH_2O16% 24h	***
C_{death} 48h vs CH_2O16% 48h	***

I. Statistic MTT data of Au@CT in the L929 cells.

Au@CT (µM)	
12.5 24h vs C_{death} 24h	***
12.5 24h vs C_{death} 48h	****
12.5 48h vs C_{death} 24h	***
12.5 48h vs C_{death} 48h	****
2.5 24h vs C_{death} 24h	****
2.5 24h vs C_{death} 48h	****
2.5 48h vs C_{death} 24h	****
2.5 48h vs C_{death} 48h	****
1.25 24h vs C_{death} 24h	****
1.25 24h vs C_{death} 48h	****
1.25 48h vs C_{death} 24h	****
1.25 48h vs C_{death} 48h	****
C_{death} 24h vs CH_2O16% 24h	***
C_{death} 24h vs CH_2O16% 48h	***
C_{death} 48h vs CH_2O16% 24h	****
C_{death} 48h vs CH_2O16% 48h	****

J. Statistics wound-healing data for post-incubation of CB extract in BJ-5ta cells. The rest of the data did not present significant differences.

CB Extract (g/mL)		
10h	Control vs CBC1	*
14h	Control vs CBC1	*
18h	Control vs CBC1	**
22h	Control vs CBC1	*

K. Statistics wound-healing data for post-incubation of CT extract in BJ-5ta cells. The rest of the data did not present significant differences.

CT Extract (g/mL)		
10h	Control vs CTC1	*
	Control vs CTC2	**
14h	Control vs CTC2	*
18h	Control vs CTC1	*
	Control vs CTC2	***
22h	Control vs CTC2	**
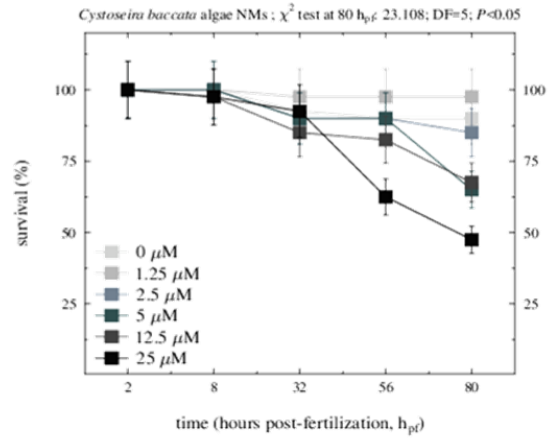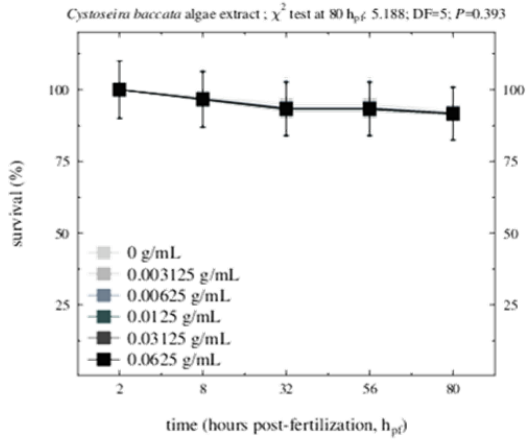
a. Survival statistic data of *CB* extract and Au@CB.
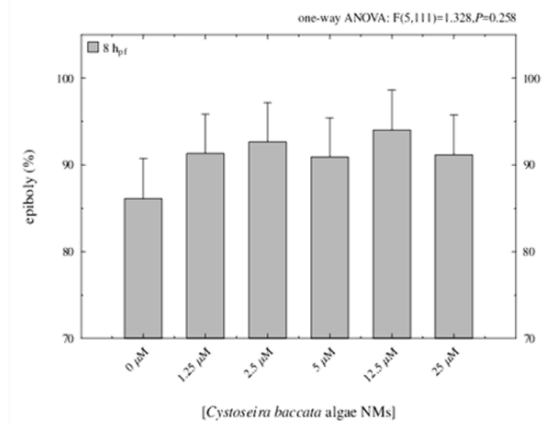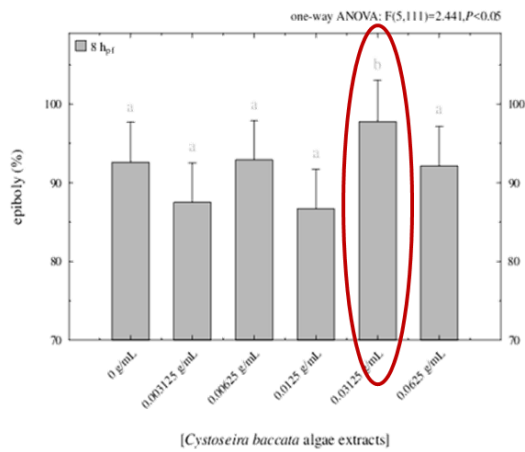
b. Epiboly statistic data of *CB* extract and Au@CB.
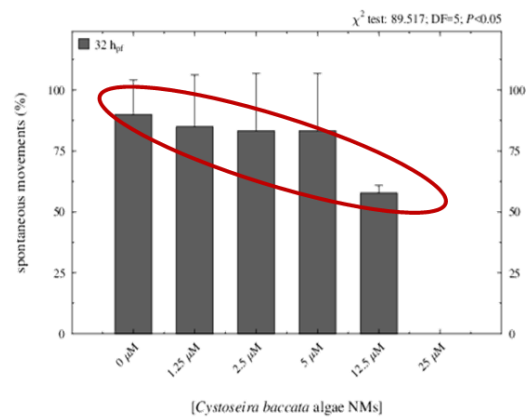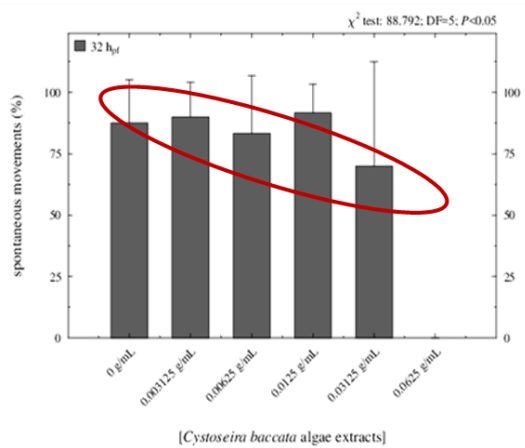
c. -Spontaneous movements statistic data of CB extract and Au@CB.
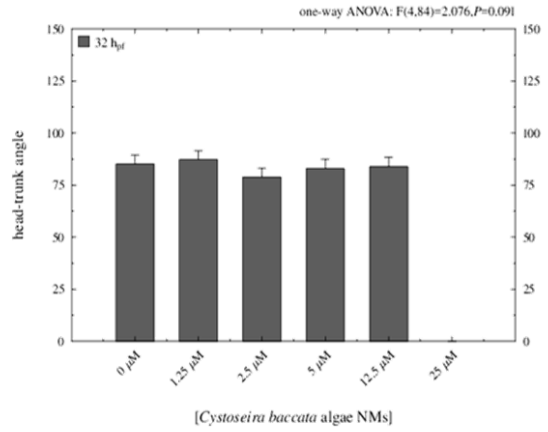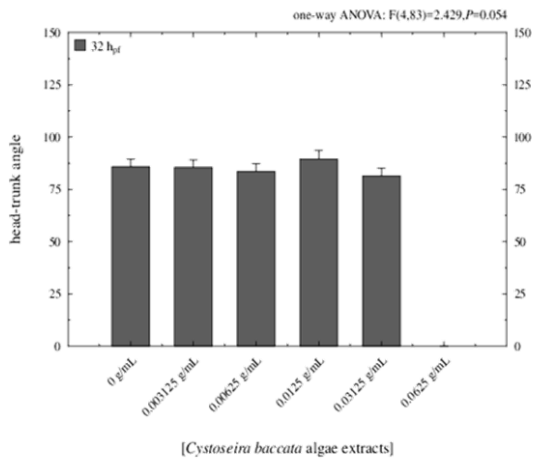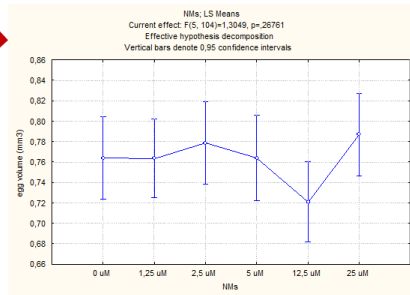
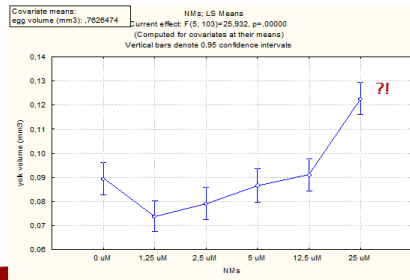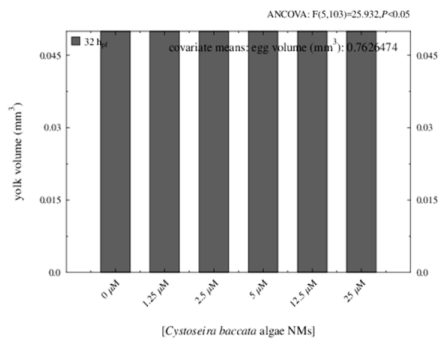d. -Head-trunk angle statistic data of CB extract and Au@CB.
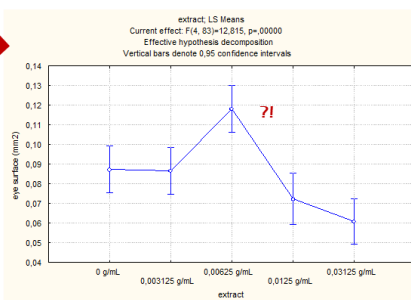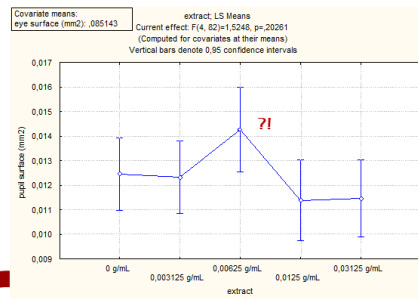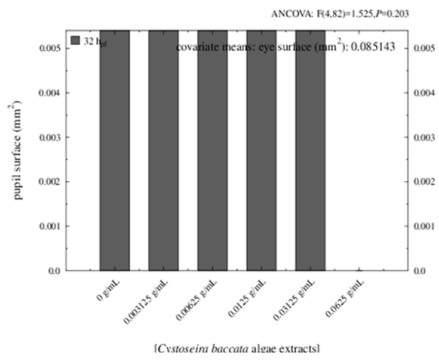
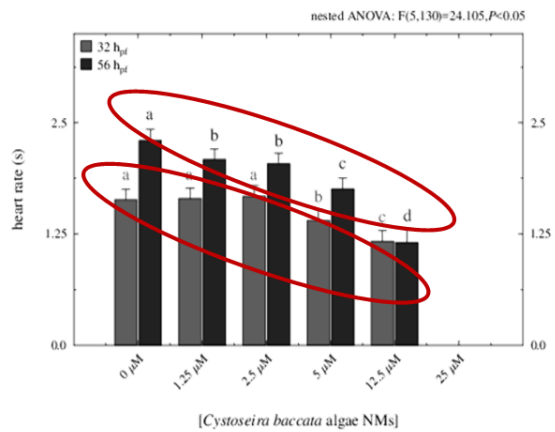e. Pupil surface statistic data of CB extract.
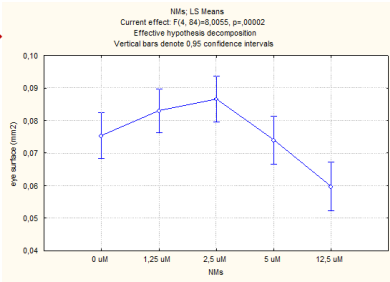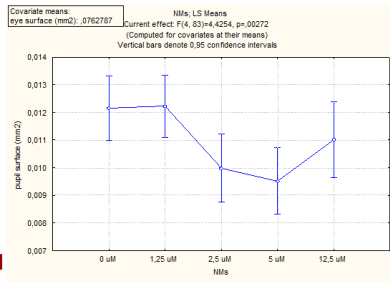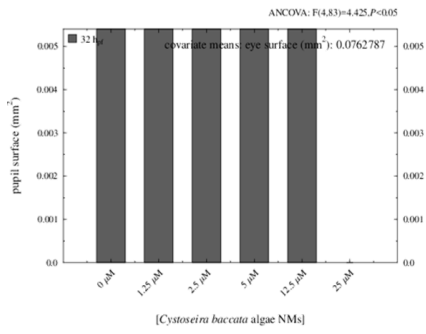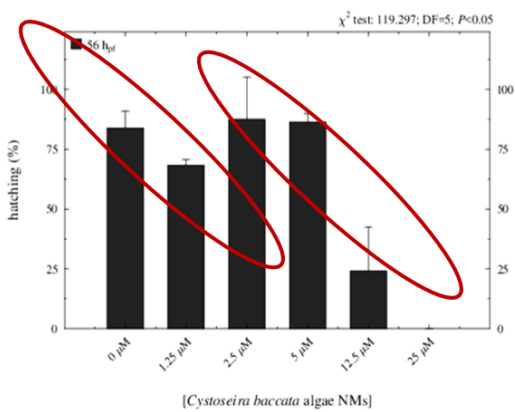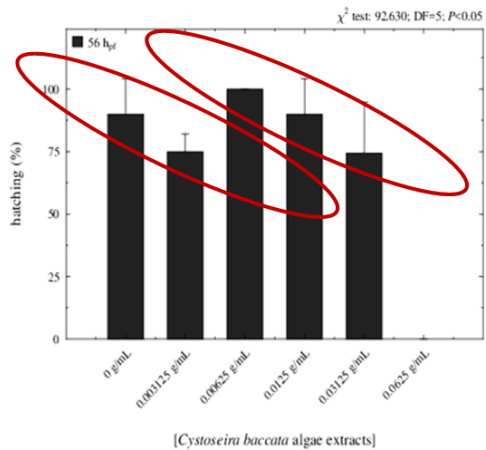
f.   Pupil surface statistic data of Au@CB.
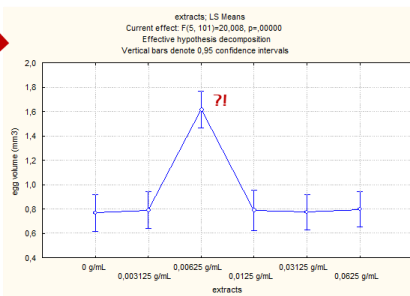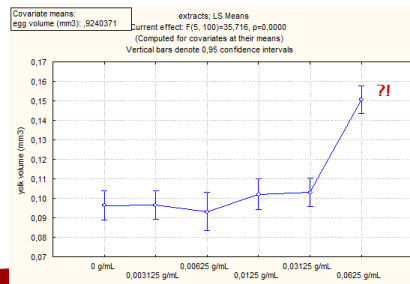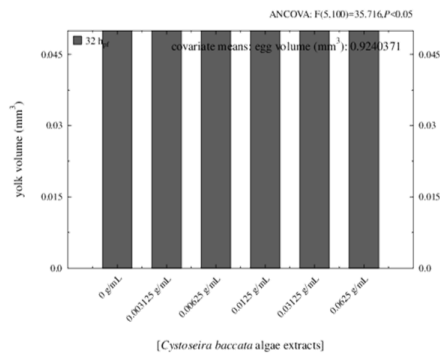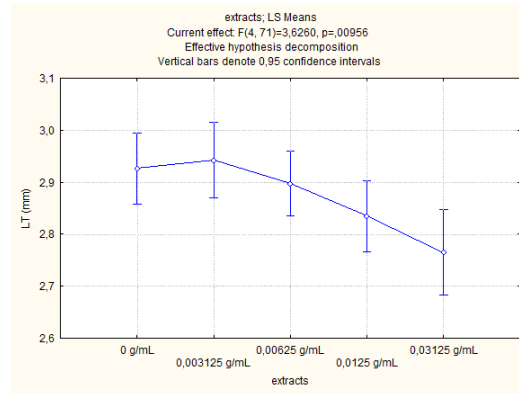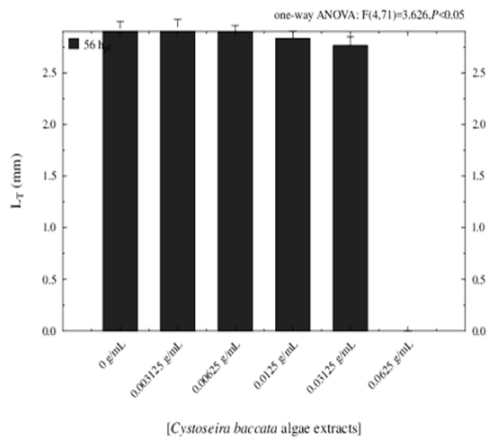

g.   Yolk volume statistic data of CB extract.

ANCOVA: F(5,103)=25.932,*P*<0.05

Covariate means:
egg volume (mm3): ,7626474

NMs; LS Means
Current effect: F(5, 103)=25.932, p=,00000
(Computed for covariates at their means)
Vertical bars denote 0,95 confidence intervals

NMs; LS Means
Current effect: F(5, 104)=1,3049, p=,26761
Effective hypothesis decomposition
Vertical bars denote 0,95 confidence intervals

h.   -Yolk volume statistic data of Au@CB.

nested ANOVA: F(5,122)=78.028,*P*<0.05

nested ANOVA: F(5,130)=24.105,*P*<0.05
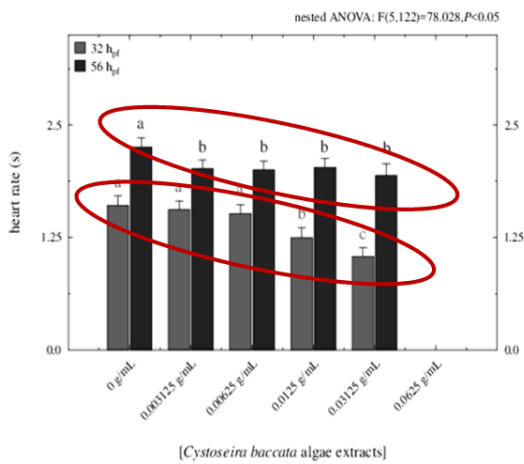
i.   Heart rate (at 32 h_{pf} and 56 h_{pf}) statistic data of CB extract and Au@CB.

χ^2 test: 92.630; DF=5; *P*<0.05

χ^2 test: 119.297; DF=5; *P*<0.05

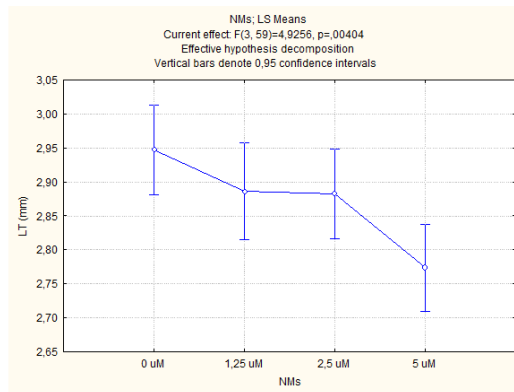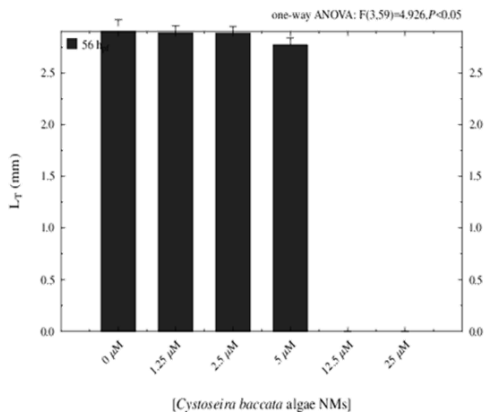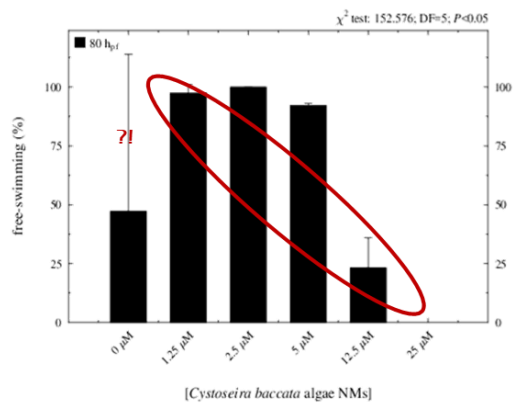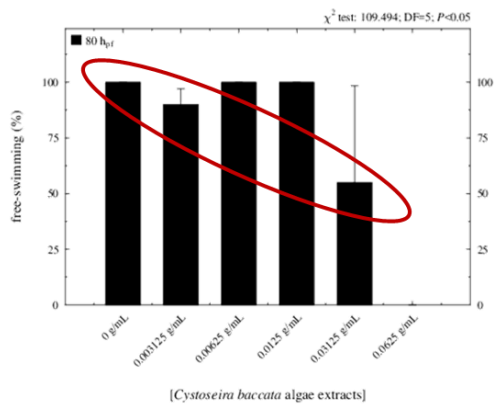j.   -Hatching statistic data of CB extract and Au@CB.
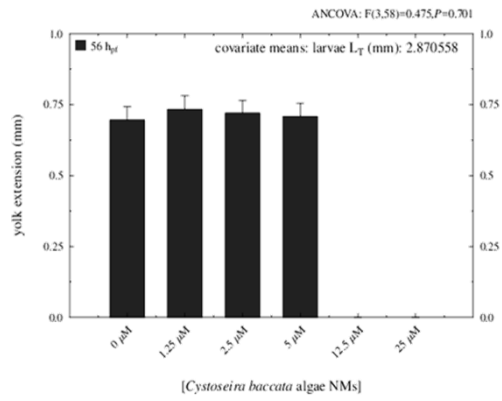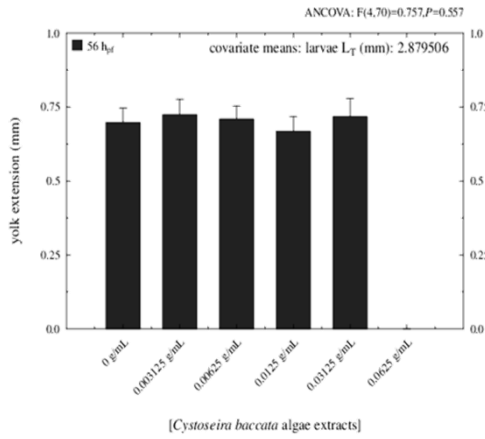
k. Yolk extension statistic data of CB extract and Au@CB.

l. L$_T$ statistic data of CB extract.

m. L$_T$ statistic data of Au@CB.

n. Free-swimming statistic data of CB extract and Au@CB.